

# Méthodes pour l'automatisation de la dosimetrie en radiothérapie.

*Methods for automatization of radiotherapy dosimetry.*

Thèse de doctorat de l'université Paris-Saclay

Spécialité de doctorat: ...

École doctorale n° 573 Interfaces : matériaux, systèmes, usages, ED INTERFACE  
Graduate School: Sciences de l'Ingénierie et des Systèmes, SIS

Thèse préparée dans les unités de recherche **Radiothérapie** (Institut Régionale du Cancer de Montpellier), **Advanced Research** (TheraPanacea), et **MICS, Mathématiques et Informatique pour la Complexité et les Systèmes** (Université Paris-Saclay, CentraleSupélec) , sous la direction de **Nikos Paragios**, Professeur, et la co-direction de **Paul-Henry Cournède**, Professeur

Thèse soutenue à Paris-Saclay, le JJ mois AAAA, par

**Paul Raymond François DUBOIS**

## Composition du jury

Membres du jury avec voix délibérative

<b>Eric DEUTCH</b> Titre, Affiliation	Président
<b>Daniela THORWARTH</b> Titre, Affiliation	Rapporteur & Examinatrice
<b>Vincent LEPETIT</b> Titre, Affiliation	Rapporteur & Examinateur
<b>Erik ENGWALL</b> Titre, Affiliation	Examinateur
<b>Pascal FENOGLIETTO</b> Titre, Affiliation	Examinateur
<b>Paul-Henry COURNÈDE</b> Titre, Affiliation	Examinateur
<b>Nikos PARAGIOS</b> Titre, Affiliation	Examinateur

**Titre:** Méthodes pour l'automatisation de la dosimétrie en radiothérapie.

**Mots clés:** Mathématiques, Intelligence Artificielle, Radiothérapie

**Résumé:**

La dosimétrie en radiothérapie est essentielle pour garantir la précision et la sécurité des traitements contre le cancer. La complexité et la variabilité de la planification des traitements nécessitent des méthodologies avancées pour l'automatisation et l'optimisation. Cette thèse présente des approches novatrices visant à automatiser le processus de dosimétrie en radiothérapie.

Cette thèse commence par le développement d'un moteur de dosimétrie et une évaluation approfondie des algorithmes d'optimisation open-source existants pour la planification des traitements. Ensuite, ce manuscrit analyse les relations entre différentes doses. Cette analyse conduit à la proposition d'un cadre novateur pour l'optimisation multi-objectif et la sélection robuste de plans à l'aide de la théorie des graphes.

Afin de réduire davantage le temps nécessaire pour la planification en radiothérapie, la thèse explore l'application de l'apprentissage par renforcement pour l'optimisation des doses. Le système proposé réalise la dosimétrie pour de nouveaux patients en exploitant les données de dose

des patients traités dans le passé. Cette méthode entièrement automatisée peut s'adapter aux pratiques de différentes cliniques, réduisant ainsi le besoin d'ajustements manuels et facilitant son adoption en pratique.

De plus, la thèse examine l'utilisation de l'apprentissage profond pour la prédiction des doses, en proposant une série de modèles guidés par des Histogrammes Dose-Volume (DVH) cibles. Ce guidage orientation permet l'incorporation de directives lors de la génération de doses par les modèles. En outre, cette technique permet d'entraîner un seul modèle capable de s'adapter, plutôt qu'un modèle pour chaque clinique.

Les contributions de cette thèse présentent des avancées dans la dosimétrie en radiothérapie, ouvrant la voie au développement d'un système de planification de traitement entièrement automatisé, s'adaptant aux contraintes cliniques, conçu pour fonctionner avec une e. Ces innovations pourraient améliorer les flux de travail cliniques, en réduisant l'intervention humaine à un minimum, rendant la radiothérapie plus efficiente.

**Title:** Methods for automatization of radiotherapy dosimetry.

**Keywords:** Mathematics, Artificial Intelligence, Radiotherapy

**Abstract:**

Radiotherapy dosimetry is critical in ensuring the precision and safety of cancer treatments. The complexity and variability of treatment planning necessitate advanced methodologies for automation and optimization. This thesis introduces novel approaches aimed at automating the radiotherapy dosimetry process.

The research begins with developing a dosimetry engine, and comprehensively evaluating existing open-source optimization algorithms for treatment plannification. Then, this thesis analyzes the relationships between different treatment plans. This analysis leads to the proposal of a novel framework for multi-objective optimization and robust plan selection using graph theory.

To further reduce the time required for radiotherapy planning, the thesis explores the application of reinforcement learning for dose optimization. The proposed system performs

dosimetry for new patients by leveraging dose data from past patients. This fully automated method can adapt to clinical dependencies, reducing the need for manual fine-tuning and easing its adoption in practice.

In addition, the thesis investigates the use of deep learning for dose prediction, proposing a series of models guided by target Dose Volume Histograms (DVH). This guidance facilitates the incorporation of guidelines into the deep-generated doses. Moreover, it allows a single model to be trained instead of one for each clinic.

The contributions of this thesis represent advancements in radiotherapy dosimetry, paving the way for the development of a fully automated, clinically dependent treatment planning system designed to operate with minimal human intervention. These innovations could enhance clinical workflows, making radiotherapy more efficient.

## Acknowledgments

During those three years, I often felt alone, but I eventually realized that I couldn't name people who supported me, not because there were too few, but because there were so many. This section is dedicated to all those who indirectly contributed to this manuscript.

[...]



# List of Contributions

- Teaching: *Consistency and Reproducibility of Grades in Higher Education: A Case Study in Deep Learning*
- ArXiV: Radiotherapy Dosimetry: A Review on Open-Source Optimizer
- ESTRO: A Novel Framework for Multi-Objective Optimization and Robust Plan Selection Using Graph Theory
- SFPM: Dose Volume Histograms Guided Deep Dose Predictions
- AIME: Radiotherapy Dose Optimization via Clinical Knowledge Based Reinforcement Learning (conference + full paper)
- ASTRO: Clinically Dependent Fully Automatic Treatment Planning System
- SFRO: Attention Mechanism on Dose-Volume Histograms for Deep Dose Predictions



# List of Figures

1.1	Diagrams of photon interactions with matter observed in the kilo and mega-voltage energy range.	9
1.2	Quality of the DNA in healthy and tumor cell after radiotherapy sessions.	10
1.3	Typical radiotherapy patient path.	13
1.4	MLC-LINAC Machines Irradiation Filtering System.	15
1.5	Example of a fluence map discretization.	18
1.6	Example of level set matching with leaves.	19
1.7	MLC leaves can not always be set to shape level sets of fluence functions.	19
1.8	Example of a fluence map segmentation along a leaf pair axis.	20
1.9	Fluence curve can be approximated with arbitrary error.	21
3.1	Example of a fluence discretized to $20 \times 20$ bixels.	32
3.2	Organs functioning types.	34
3.3	Irradiation type survival of organs serial-like and parallel-like.	36
3.5	Typical penalization of a dose on an OAR according to the maximal dose constraint $D_{20\%} \leq 25$ Gy.	38
3.6	Evolution of the objective function value ('cost') through optimization iterations and computation time for four typical dosimetry cases.	43
4.1	Example of two doses that have the same clinical effect (measured from the DVHs), but very different voxel-wise dose values.	48
4.2	DVHs: Comparison of classical and flipped axes styles.	53
4.3	Pairwise distances between doses (with different distances calculation method)	54
4.4	Comparing Distances	56



## List of Tables



# Contents

<b>1</b>	<b>Background</b>	<b>1</b>
1.1	Medical context . . . . .	4
1.2	Physics of Radiotherapy . . . . .	7
1.3	Biological effect on cells . . . . .	10
1.4	Patient Path . . . . .	12
1.5	Machines . . . . .	14
1.6	Irradiations techniques . . . . .	16
1.7	Dosimetry steps . . . . .	17
1.8	Simulation . . . . .	22
1.9	Treatment Planning Systems . . . . .	22
<b>2</b>	<b>Introduction</b>	<b>25</b>
2.1	Context . . . . .	27
2.2	Problematic . . . . .	27
2.3	State of the Art . . . . .	27
2.4	Unsolved problems . . . . .	27
2.5	Contribution . . . . .	27
<b>3</b>	<b>Dosimetry Optimization</b>	<b>29</b>
3.1	Discretization . . . . .	31
3.2	Naive Optimization Method . . . . .	33
3.3	Constraints and Importance Factors . . . . .	34
3.4	Dose Mimicking . . . . .	40
3.5	Optimization Algorithm Review for Dosimetry . . . . .	40
<b>4</b>	<b>Doses Relationship</b>	<b>45</b>
4.1	Distance Between Doses . . . . .	47
4.2	Network of Doses . . . . .	58
4.3	Novel Dosimetry Automation Approach with Graph Theory . . . . .	59
<b>5</b>	<b>Classical Dosimetry Automation</b>	<b>61</b>

5.1	Radiotherapy Dose Optimization via Clinical Knowledge Based Reinforcement Learning (AIME 2024) . . . . .	63
5.2	Clinically Dependent Fully Automatic Treatment Planning System (ASTRO 2024)	63
<b>6</b>	<b>Dosimetry Automation via Mimicking</b>	<b>65</b>
6.1	Dose-Volume Histograms Guided Deep Dose (SFPM 2024) . . . . .	67
6.2	Attention Mechanism on Dose-Volume Histograms for Deep Dose Predictions (SFRO 2024) . . . . .	67
<b>7</b>	<b>Conclusion</b>	<b>69</b>
<b>8</b>	<b>Perspectives</b>	<b>71</b>

# Background

## Abstract

The background chapter of this PhD provides a comprehensive overview of key concepts in cancer treatment and radiotherapy. If you already know about radiotherapy and multi-leaf collimator, I strongly advise to skip this chapter.

This chapter begins by outlining the nature of cancer, its phases, stages, risk factors, and common types of treatments (with their advantages and disadvantages). Then, the physics of radiotherapy is explored, with a focus on ionizing radiation, and biological effects of radiation. This chapter also presents the patient journey in radiotherapy, from diagnosis and treatment prescription to planning and follow-up. Key technologies used in radiation therapy, such as multi-leaf collimator (MLC) linear accelerator (LINAC) are introduced. Lastly, this chapter covers the irradiation techniques, and details major steps in the dosimetry process: beam orientation optimization (BOO), fluence map optimization (FMO), leaf sequencing (LS), and direct aperture optimization (DAO).

1.1	Medical context . . . . .	4
1.1.1	About cancer . . . . .	4
1.1.2	Treatment types . . . . .	5
1.2	Physics of Radiotherapy . . . . .	7
1.2.1	Ionizing radiation . . . . .	7
1.2.2	Photon interactions . . . . .	8
1.2.3	Photon attenuation . . . . .	8
1.3	Biological effect on cells . . . . .	10
1.3.1	Radiation effects on DNA . . . . .	10
1.3.2	Radiation affects the plasma membrane . . . . .	11
1.3.3	Radiations and cell organelles performances . . . . .	11
1.3.4	Radiation alters the biological behavior of cells . . . . .	11
1.3.5	Radiation effects when combined with immunotherapy . . . . .	11
1.4	Patient Path . . . . .	12
1.4.1	Diagnostic . . . . .	13
1.4.2	Radiotherapy Prescription . . . . .	13
1.4.3	CT scan and Contouring . . . . .	13
1.4.4	Treatment Planning . . . . .	13
1.4.5	Irradiation Sessions . . . . .	14
1.4.6	Follow-up . . . . .	14
1.5	Machines . . . . .	14
1.5.1	Molds . . . . .	14
1.5.2	MLC-LINAC . . . . .	15
1.5.3	Tomotherapy . . . . .	15
1.5.4	CyberKnife . . . . .	15
1.5.5	Brachytherapy . . . . .	16
1.6	Irradiations techniques . . . . .	16
1.6.1	3D-CRT . . . . .	16
1.6.2	IMRT . . . . .	16
1.6.3	VMAT . . . . .	17
1.7	Dosimetry steps . . . . .	17
1.7.1	BOO . . . . .	17
1.7.2	FMO . . . . .	18
1.7.3	LS . . . . .	18
1.7.4	DAO . . . . .	20
1.8	Simulation . . . . .	22
1.9	Treatment Planning Systems . . . . .	22
1.9.1	Manufacturer . . . . .	22
1.9.2	Non-manufacturer . . . . .	23



## 1.1 Medical context

This PhD thesis is about radiation therapy (RT) for cancer treatment.

### 1.1.1 About cancer

Cancer is a complex disease that can affect many parts of the body. This malady is characterized by the uncontrolled growth of cells that can invade and destroy surrounding tissues. Cancer is a leading cause of death worldwide. In 2022, the World Health Organization (WHO) estimated 20 million new cancer cases and 9.6 million deaths linked to cancer [1]. Cancer affects about 20% of the population, and is responsible for 1 in 10 deaths.

**Cancer characteristics** Cancer is characterized in various manners, starting with an cell proliferation. Cancerous cells reprogram cellular metabolism to support their growth [9], they can also stop cell growth arrest mechanisms, and usually manage to evade apoptosis (programmed cell death). Cancer cells can escape the immune system, and change their cellular response phenotypic via plasticity. At some point, cancer cells can get the ability to undergo a sufficient number of successive cell cycles of growth and division to generate macroscopic tumors. To support their growth, they create new blood vessels to get nutrients. Finally, they can escape and form metastasis, and will eventually provoke senescence<sup>1</sup>.

**Conditions leading to cancer** Cancer is a complex disease. First, cancer is caused by mutations in the DNA. These mutations can be inherited or acquired. Second, cancer is embraced by epigenetic reprogramming, i.e., gene expression changes (not caused by changes in the DNA sequence). Third, cancer is often associated with an inflammatory context; inflammation can promote cancer growth and spread. Finally, cancer is often associated with a disruption of the microbiota (the microbial community living in and on the human body). This disruption can promote cancer growth and spread.

**Phases of cancer** Cancer develops in several phases.

**Initiation** The first phase is initiation: Mutations in the DNA transform a healthy cell into a cancer cell.

**Promotion** The second phase is promotion or "tumorigenesis". During this phase, the cancer cell grows and divides uncontrollably to form a tumor cluster of cells. This growth is promoted by changes in gene expression and other factors [60]. It may also create new blood vessels to get nutrients and oxygen.

---

<sup>1</sup>deterioration of functional characteristics

**Evolution** The final phase is evolution. The tumor will first grow locally, then regionally, invading and damaging surrounding tissues. Finally, the cancer cell will spread to other body parts, forming metastasis. Metastasis is the leading cause of death in cancer patients [51].

**Cancer stages** Cancer is classified into stages [2].

- Stage 0: 'in situ neoplasm'; it means a group of abnormal cells in an area of the body. The cells may develop into cancer in the future.
- Stage 1: the cancer is small and contained within the organ it started in.
- Stage 2: the tumor is larger than in stage 1, but the cancer hasn't started to spread into the surrounding tissues.
- Stage 3: the cancer is larger; it has started to spread into surrounding tissues and cancer cells in the lymph nodes nearby.
- Stage 4: the cancer has spread from where it started to another body organ. This spread is also called secondary or metastatic cancer.

Doctors use the TNM system to describe the cancer stage [26].

T stands for the size of the Tumour; it can be 1, 2, 3, or 4, with one being small and four being large.

N stands for the number of lymph Nodes affected; it can be between 0 and 3. 0 means no lymph node contains cancer cells; 3 means many lymph nodes contain cancer cells.

M stands for the existence of Metastasis in another part of the body; it can be 0 (no spread) or 1 (cancer has spread).

**Most common cancers** According to the WHO, the most common cancers are lung, breast, colorectal, prostate, skin, and stomach cancer. This thesis mainly focuses on prostate cancer, which is among the most common ones.

**Risk factors** Tobacco use, alcohol consumption, unhealthy diet, physical inactivity, and air pollution are risk factors for other cancer types. However, the leading risk factor for prostate cancer is age. Thus, it touches all social populations evenly and is unavoidable.

### 1.1.2 Treatment types

There are three main types of cancer treatment: surgery, radiation therapy, and chemotherapy. The choice of treatment depends on the type and stage of cancer, the patient's age and general health, and other factors.

### 1.1.2.1 Surgery

Surgery is the most effective cancer treatment [31]. It involves removing the tumor and surrounding tissue. Surgery is often used to treat early-stage cancer that has not spread to other parts of the body. For surgery to be possible, the tumor must be located in a place the surgeon can easily access. Surgery can be followed by other treatments, such as radiation therapy or chemotherapy, to kill any remaining cancer cells.

**Advantages** Surgery is considered a curative treatment modality; cancerous tissues are entirely removed, leading to disease eradication. Being a localized intervention, it primarily affects the targeted area with minimal systemic side effects. Additionally, surgical procedures are typically performed in a single session, unlike other treatment modalities (e.g., radiotherapy) that may require multiple cycles.

**Disadvantages** Surgery is invasive, and it can be painful. The main disadvantage, is that it can only be used for localized cancer (with no metastasis) accessible to the surgeon.

### 1.1.2.2 Chemotherapy

Chemotherapy is a treatment that uses drugs to kill cancer cells. It is systemic, meaning it can reach cancer cells anywhere in the body. Therefore, it usually has strong side effects. Chemotherapy is often used to treat cancer that has spread to multiple parts of the body (i.e., metastatic cancer).

Depending on how advanced the cancer is, chemotherapy can be used to cure, control, or relieve symptoms (palliation).

**Advantages** Chemotherapy can be used to treat cancer that has spread to multiple parts of the body. It can also be used to relieve symptoms and improve quality of life.

**Disadvantages** Chemotherapy is a heavy treatment, with strong side effects. It can also weaken the immune system, making the patient more prone to infections. Finally, newer drugs tend to be very expensive.

### 1.1.2.3 Radiation therapy

Radiation therapy is a treatment that uses high-energy radiation to kill cancer cells. It is semi-local, meaning that it only affects the tumor, and the tissues traversed by the radiation beams [54]. Radiation therapy is curative most of the time. It can be used alone or in combination with other treatments.

Radiation therapy can be delivered in two ways: external radiation therapy and internal radiation therapy. External radiation therapy uses a machine to deliver radiation to the tumor from

outside the body. Internal radiation therapy uses radioactive materials placed directly into or near the tumor. This thesis focuses on external radiation therapy.

**Advantages** Radiation therapy is a non-invasive treatment, with limited side effects. It is relatively localized, and can be used to treat cancers that are not accessible via surgery.

**Disadvantages** Radiation therapy still targets healthy cells. Depending on the patient's response, it may cause side effects.

#### 1.1.2.4 Other treatments

Cancer research is very active, and new treatments are constantly being developed. These treatments are often used in combination with others.

**Immunotherapy** Immunotherapy is a treatment that uses the body's immune system to fight cancer. It can boost or change how the immune system works to find and attack cancer cells. It is a systemic treatment.

**Targeted therapy** Targeted therapy is a treatment that uses drugs to target specific molecules that are involved in cancer growth. It is a systemic treatment.

**Hormone therapy** Hormones are proteins or substances the body makes that help control how specific cell types work. Hormone therapy is a treatment that uses drugs to block or lower the amount of hormones in the body that are involved in cancer growth. It is a systemic treatment.

**Stem cell transplant** A stem cell transplant is a treatment that uses stem cells to replace cells damaged or destroyed by cancer treatment. It is a systemic treatment.

## 1.2 Physics of Radiotherapy

Radiation therapy uses high-energy radiation to kill cancer cells.

### 1.2.1 Ionizing radiation

Ionizing radiation has enough energy to remove tightly bound electrons from atoms, creating ions. X-rays and gamma rays are both electromagnetic radiations that are ionizing and high-energy photons. Some particle radiations, such as particles, beta particles, and neutrons, are also ionizing, but radiotherapy uses photon radiations.

X-rays are produced by accelerating electrons to collide with a target material and are used in medical imaging and (external) radiation therapy. In contrast, gamma rays originate from the radioactive decay of specific atomic nuclei and are used in (internal) radiation therapy.

Because ionizing radiation therapy can damage the DNA in cells and lead to cell death, it is used in radiation therapy for treating cancer.

### 1.2.2 Photon interactions

Photon-matter interactions within an absorbing medium undergo stochastic (i.e., random) processes. Four types of interactions (figure 1.1) are possible for photons; their occurrence depends on the atomic number, matter, and the energy of the incident photon [15]. Three of the four interactions generate secondary ionizing particles that deposit energy in the medium.

**Rayleigh scattering** The Rayleigh scattering (figure 1.1a) does not change the energy of the incident photons and consequently has no direct consequence on the body. Rayleigh scattering predominantly occurs with low-energy photons (typically  $< 100$  keV).

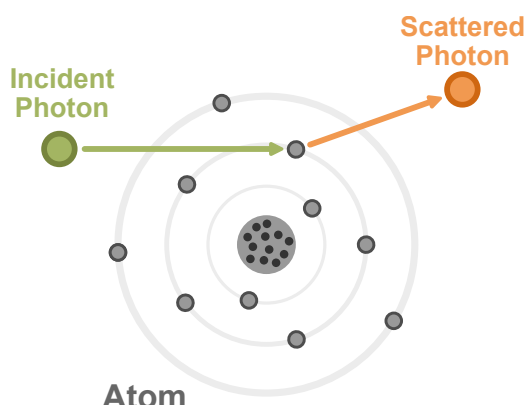
**Photoelectric absorption** The photoelectric absorption effect (figure 1.1b) is the process by which an atom absorbs a photon, and an electron is ejected from the atom. The photon ceases to exist, and its energy is transferred to the electron. The ejected electron, called a photoelectron, can ionize other atoms, leading to dose deposition. The photoelectric effect is the dominant interaction for low-energy ( $< 100$  keV) photons.

**Compton scattering** Compton scattering (figure 1.1c) is the process by which an atom scatters a photon, and ejects an electron from the atom. The photon is scattered at an angle, and part of its energy is transferred to the electron. The emitted electron is called a Compton electron, which can ionize other atoms, leading to dose deposition. Compton scattering is the dominant interaction for medium-energy ( $\approx 0.1$  to  $\approx 10$  MeV) photons.

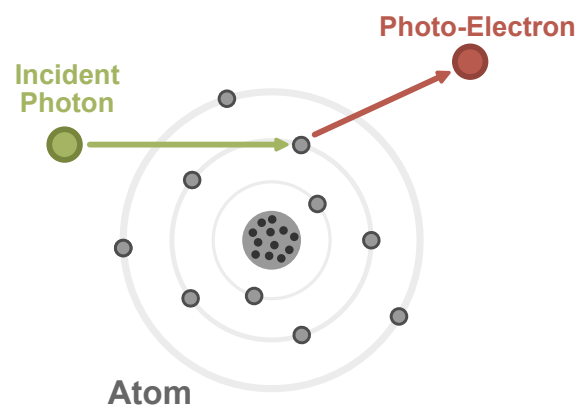
**Pair production** Pair production (figure 1.1d) is when an atomic nucleus absorbs a photon and creates an electron-positron pair. The photon ceases to exist, and its energy is transferred to the electron-positron pair. The positron rapidly interacts with another electron of the matter, producing two photons emitted at  $180^\circ$  from each other. The electron can ionize other atoms, leading to dose deposition. Pair production is the dominant interaction for high-energy ( $> 10$  MeV) photons.

### 1.2.3 Photon attenuation

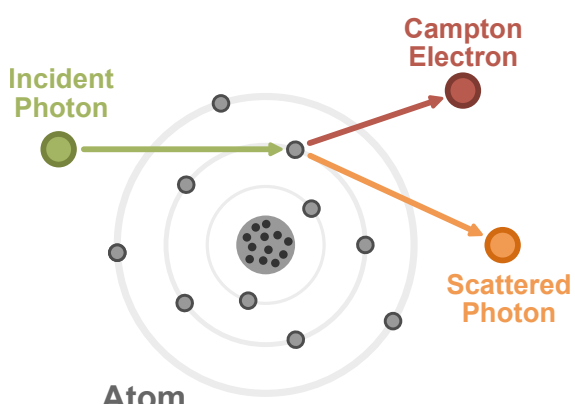
The photon beam will be attenuated as it passes through the medium, and its intensity will decrease. The dose deposition in the medium is proportional to the intensity of the photon



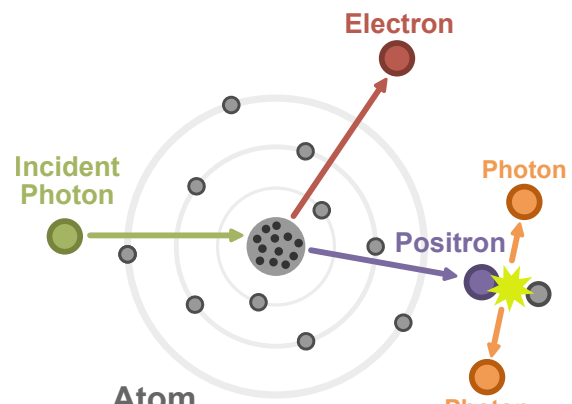
(a) Diagram of Rayleigh Diffusion.



(b) Diagram of Photoelectric Absorption.



(c) Diagram of Compton Scattering.



(d) Diagram of Pair Production.

Figure 1.1: Diagrams of photon interactions with matter observed in the kilo and mega-voltage energy range.

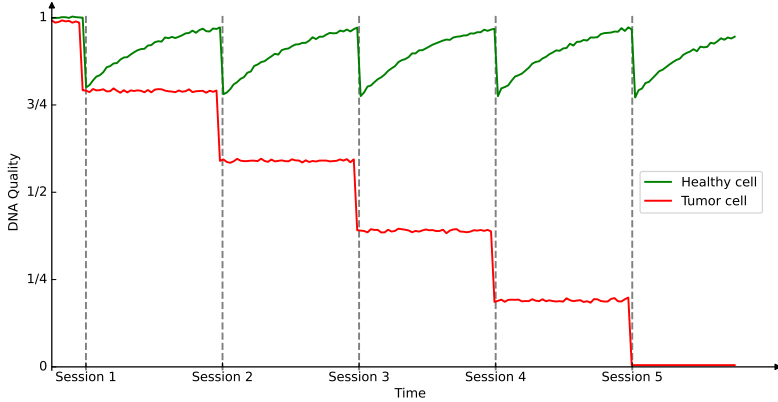


Figure 1.2: Quality of the the DNA in healthy and tumor cell after radiotherapy sessions.

beam. The attenuation of the beam follows an exponential law concerning the depth of the medium traversed (Lambert-Beer law) [5]:

$$I(x) = I_0 \exp(-\mu x)$$

where  $I$  is the intensity of the photon beam after passing through a thickness  $x$  of the medium,  $I_0$  is the initial intensity of the photon beam, and  $\mu$  is the attenuation coefficient of the medium.

## 1.3 Biological effect on cells

Ionizing radiation can damage the cells leading to cell death in various ways.

### 1.3.1 Radiation effects on DNA

Ionizing radiation damages the DNA [49] in cells and leads to cell apoptosis<sup>2</sup>, necrosis<sup>3</sup>, or senescence. Radiation induces DNA damage through both direct and indirect mechanisms: Directly, it causes single-strand breaks (SSBs), double-strand breaks (DSBs) [48], DNA crosslinks, and DNA-protein crosslinks [41]. Indirectly, radiation generates reactive oxygen species (ROS) and reactive nitrogen species (RNS), further contributing to DNA damage.

**DNA repair** Cells have mechanisms to repair DNA damage. There are several types of DNA repair mechanisms, including base excision repair (BER), nucleotide excision repair (NER), mismatch repair (MMR), and double-strand break repair (DSBR). Cancer cells often have defects in DNA repair mechanisms, making them more sensitive to radiation therapy [26]. This repair mechanism being available only for healthy cells leads to cell death only for cancerous cells when their DNA is too damaged to survive (see figure 1.2).

<sup>2</sup>process of programmed cell death

<sup>3</sup>death of most or all of the cells in an organ or tissue

### 1.3.2 Radiation affects the plasma membrane

Radiation significantly impacts the biological properties of the plasma membrane by affecting its composition, structural integrity, and functional capabilities. Radiation exposure can alter the fluidity and permeability of the cell membrane, affecting the transport of ions and molecules into and out of the cell. Additionally, radiation causes corrosive damage, and damage to the membrane can initiate signaling events that are important for the apoptotic response [11]. These changes can have cascading effects on various cellular processes, highlighting the critical role of the plasma membrane in maintaining cellular homeostasis under stress conditions.

### 1.3.3 Radiations and cell organelles performances

Radiation exerts significant detrimental effects on various cellular organelles, impacting their functionality and overall cellular health [50]. One critical target of radiation damage is the endoplasmic reticulum, where radiation can disrupt protein folding and processing, leading to cellular stress and apoptosis. Additionally, ionizing radiation induces alterations in ribosomal structure and function, impairing protein synthesis and compromising cellular homeostasis. Mitochondria, the cell's powerhouses, also exhibit altered behavior following radiation exposure, including disruptions in energy production and initiating apoptotic pathways. Furthermore, lysosomes, essential for cellular waste processing and recycling, suffer damage upon irradiation, potentially accumulating cellular debris and impairing cell function. These collective effects highlight radiation's broad and profound impact on cellular organelle performance [59].

### 1.3.4 Radiation alters the biological behavior of cells

Radiation profoundly influences the biological behavior of tumor cells and the immune system, impacting critical aspects of cancer progression and immune response. It affects tumor cell proliferation, often reducing the ability of cancer cells to multiply by damaging their DNA and cellular structures. Radiation also influences tumor cells' invasion and metastasis potential either by directly impairing their motility or altering the tumor microenvironment to make it less conducive to cancer spread. Additionally, radiation can modulate cancer-promoting inflammation, either by inducing pro-inflammatory signals that support tumor growth or by disrupting the inflammatory milieu to hinder cancer progression.

### 1.3.5 Radiation effects when combined with immunotherapy

Radiation can be used alongside immunotherapy. The effect of both treatments is more significant than the sum of their impact if used alone.

**Ray-Enhanced Anti-CTLA-4 Immunotherapy** Radiation therapy can enhance the efficacy of immune checkpoints<sup>4</sup> based therapy, such as anti-CTLA-4 immunotherapy<sup>5</sup>, a treatment that blocks the CTLA-4 protein in T cells, thus boosting the immune system's response against cancer cells. The combination of radiation and anti-CTLA-4 immunotherapy has shown promising results, as radiation-induced tumor cell death releases antigens that can further stimulate the immune system [55]. This synergy can improve tumor control and potentially better clinical outcomes than either treatment alone.

**Radiation Combined with Anti-PD-1/PD-L1 Immunotherapy** Combining radiation with anti-PD-1/PD-L1 immunotherapy<sup>6</sup> has shown significant success. Anti-PD-1/PD-L1 therapies block the PD-1/PD-L1 pathway, which tumors exploit to evade immune detection. Radiation therapy can augment this effect by increasing the immunogenicity of the tumor, thereby making cancer cells more susceptible to immune attack [19].

**TLR-Mediated Immunologic Effects of Radiation Therapy** Radiation therapy can also exert immunologic effects through Toll-like receptors (TLRs), a class of proteins involved in pathogen recognition and activation of innate immunity. Radiation can activate TLRs on immune cells, producing cytokines and chemokines that enhance the immune response against tumors. This TLR-mediated effect contributes to the synergy between radiation and immunotherapies, leading to more robust anti-tumor responses [58].

While this thesis does not focus on biological aspects, one should remember that radiation affects cells in various ways, and cancer therapy is complex.

## 1.4 Patient Path

The radiotherapy patient path encompasses several critical stages, each essential for the effective treatment of cancer. This section outlines the sequential steps of radiotherapy, from initial detection and diagnosis to follow-up care.

---

<sup>4</sup>The immune checkpoints are regulators of the immune system; they prevent the immune system from attacking all cells indiscriminately. Tumor cells sometimes exploit this mechanism to evade immune surveillance.

<sup>5</sup>Cytotoxic T-lymphocyte-associated protein 4 (CTLA-4) is a protein receptor that downregulates immune responses (it acts as an "off" switch). Blocking this receptor induces lymphocyte activation and cytokine production and has an *in vivo* antitumor effect.

<sup>6</sup>Programmed cell Death protein 1 (PD-1) is a protein present on the surface of immune cells, T lymphocytes, and is a component of the immune checkpoint. The T lymphocyte can interact via PD-1 with a tumor cell presenting protein Programmed Death-Ligand 1 (PD-L1) on its surface. This interaction inactivates the T lymphocyte and consequently inactivates one of the immune system's defense mechanisms against tumor cells. Researchers have developed antibodies that bind to PD-1 or PD-L1, called anti-PD-1 or anti-PDL-1 antibodies. Blocking the immune checkpoint by preventing the interaction between PD-1/PD-L1 can lift the inactivation of the immune system, which can then fight the tumor cell again.

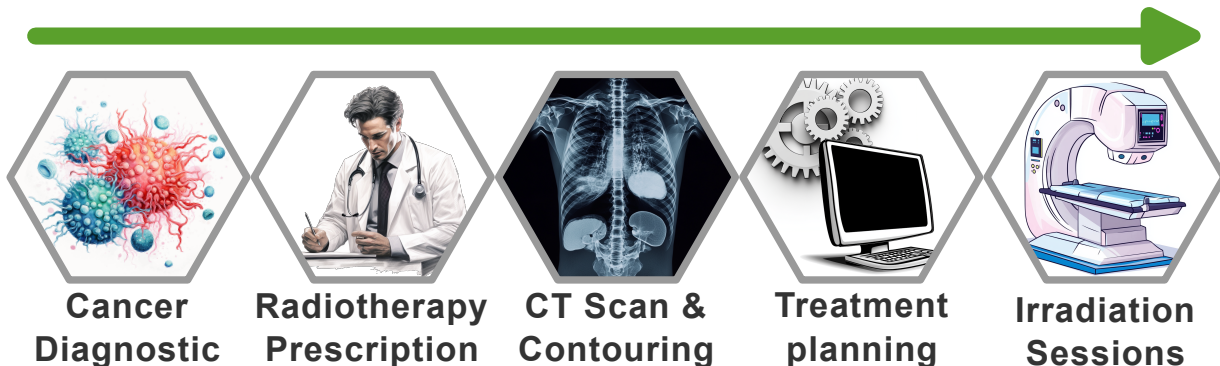


Figure 1.3: Typical radiotherapy patient path.

#### 1.4.1 Diagnostic

Patients diagnosed with a tumor can go through several paths: surgery, radiotherapy, immunotherapy, chemotherapy, or any combination. Doctors will choose the most appropriate treatment(s) based on evidence they have (biopsy, radios, et cetera). This manuscript will focus on the radiotherapy path.

#### 1.4.2 Radiotherapy Prescription

Following a confirmed diagnosis and the choice of radiotherapy treatment, the oncologist develops a prescription. This prescription specifies the type, dosage, and frequency of radiation treatment tailored to the patient's specific cancer type, location, and stage. The doctors define minimal tumor irradiation and maximum damage to surrounding healthy tissues. Most of the time, templates are used and fine-tuned to fit specific patients.

#### 1.4.3 CT scan and Contouring

A computed tomography (CT) scan is performed to obtain detailed images of the patient's anatomy. These images are used to delineate the tumor and surrounding organs at risk. Automatic segmentation delineated the contour organs on each slice. Medical doctors previously did this task, and it was heavily time-consuming. Nowadays, artificial intelligence performs with only minor human correction needed [52] [37]. After the emergence of AI for contouring, this manuscript will tackle the treatment planning problem.

The CT scan also provides the spatial information necessary for precise irradiation simulation.

#### 1.4.4 Treatment Planning

The treatment planning process involves developing a detailed plan specifying the patient's radiation dose distribution. Advanced software calculates the optimal arrangement of radiation

beams to achieve the desired dose while minimizing exposure to healthy tissues. This thesis registers new advances in the planning step. Plans must be reviewed and approved by doctors.

### 1.4.5 Irradiation Sessions

Irradiation sessions, or treatment delivery, is the actual irradiation of the patient. Cone Beam Computed Tomography (CBCT) is usually done to reposition the patient with the scan so that all organs align with the planning CT. Nowadays, the tendency is to reduce the number of irradiation sessions (the old typical five weeks of five sessions is now usually two weeks of five sessions).

### 1.4.6 Follow-up

After the completion of radiotherapy, patients enter the follow-up phase. Regular follow-up appointments are scheduled to monitor the patient's response to treatment, manage any side effects, and detect any signs of recurrence.

## 1.5 Machines

The discovery of X-rays by German physicist W. C. Roentgen in 1895 marked a pivotal moment in medical science. Only one year later, in 1896, Despeignes began using radiotherapy in France. Victor Despeignes delivered 15-30 minutes with 80 irradiation sessions (so-called "fractions") to relieve the pain of patients with stomach cancer [23].

Since then, machines have become more powerful and more complex. Modern machines can deliver mega-voltage radiation [25], which are sufficiently high to destroy tumors in minutes. However, such high-power treatments will irreversibly damage healthy tissues. Hence, as the machines became more powerful, constructors built more complex modulation mechanisms to preserve organs at risk.

### 1.5.1 Molds

The first kind of modulation used was molds: their purpose was to stop the irradiation before it reached the body. By strategically obscuring the rays, organs can be spared, as they will receive a small amount of irradiation dose, while the tumor will receive a fatal dose. Molds had significant limitations due to their single-use nature. It was necessary to create a custom mold for each patient as their anatomy differs. Typically, three molds were required for the three irradiation angles. Modern technology avoids single-use molds using motorized blockers to stop the rays and dynamically modulate the radiation beam.

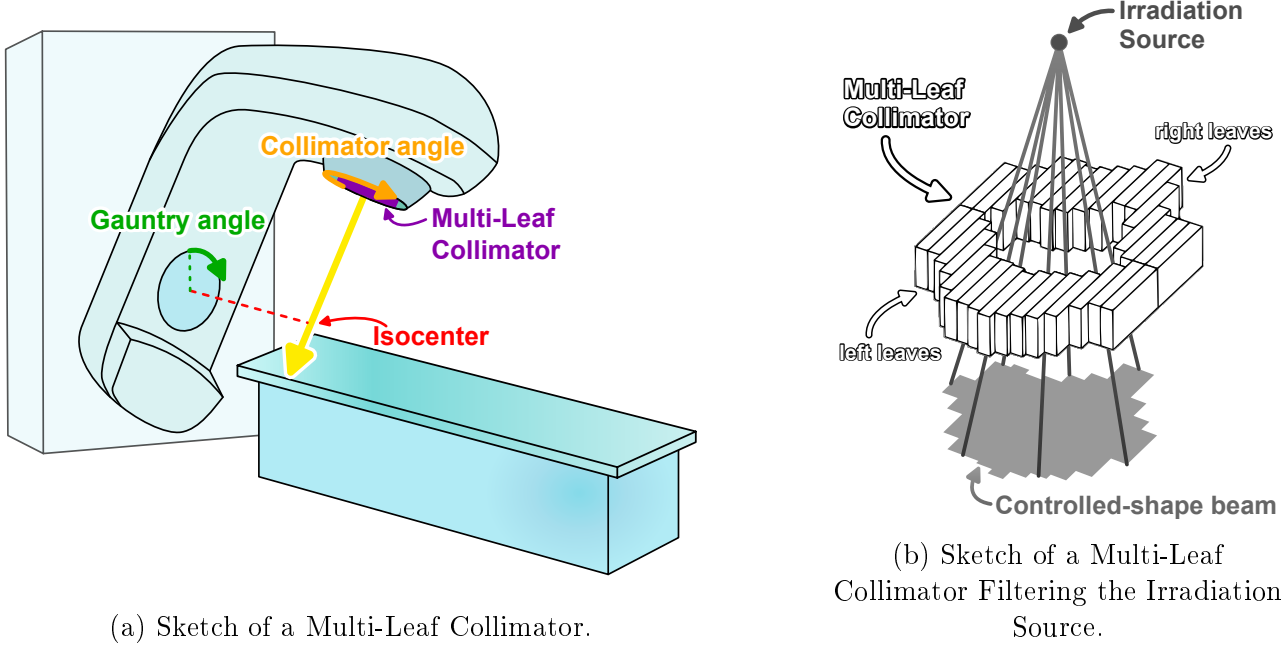


Figure 1.4: MLC-LINAC Machines Irradiation Filtering System.

### 1.5.2 Multi-Leaf Collimator - LINear ACcelerators

Multi-Leaf Collimator (MLC) technology combined with Linear Accelerators (LINAC) was a revolution in the radiotherapy world [4] [61]. They are capable of turning around the patient to deliver irradiation from multiple angles (figure 1.4a). Moreover, an array of motorized leaf pairs can shape the radiation beam with high precision (figure 1.4b). Additionally, MLC systems are sometimes equipped with jaws, which help to shape the beams better. The MLC-LINAC is the most common type of radiation therapy machine used today. This manuscript will focus on the MLC-LINAC system due to its widespread use and versatility in clinical settings.

### 1.5.3 Tomotherapy

Tomotherapy systems have an irradiation head that rapidly rotates around the patient, equipped with a single layer of binary blockers that can be activated and deactivated almost instantaneously [36]. The tomotherapy machines follow a helical path [27], rotating around the patient while simultaneously moving along their body.

### 1.5.4 CyberKnife

CyberKnife systems are another non-invasive alternative to conventional MLC-LINAC radiotherapy machines with higher flexibility [28]. These CyberKnife machines have the irradiation head mounted on a robotic arm, which allows a vast array of motions around the patient. This flexibility enables the delivery of even more complex-shaped doses. CyberKnife technology is

particularly beneficial for treating unusual tumors in challenging or sensitive body areas.

### 1.5.5 Brachytherapy

Brachytherapy involves the placement of a radioactive source directly inside the body of the patient [10]. This technique allows for delivering localized high-dose radiation. Although brachytherapy involves an invasive procedure, it significantly minimizes radiation exposure to surrounding healthy tissues. The localized character of brachytherapy makes it a good treatment option for some types of cancer.

## 1.6 Irradiations techniques

This section describes the main irradiation techniques that can be used with MLC-LINAC machines. The techniques have evolved over the years of MLC usage. Better irradiation techniques improve tumor targeting while keeping exposure of healthy tissues to a minimum.

### 1.6.1 3-Dimensional Conformal Radiotherapy

Three-Dimensional Conformal Radiotherapy (3D CRT) shapes radiation beams to closely fit the contours of the tumor. The MLC leaves are positioned to match the tumor's contour projection on a plane perpendicular to the radiation rays, typically using three angles. Such shaping of the beams can be done with mold (which is single-use) or with an MLC. Although 3D CRT targets the Principal Target Volume (PTV) more than Organs At Risk (OARs), modern techniques provide superior sparing of healthy tissues. Consequently, advanced and less naive methods have largely supplanted 3D CRT in contemporary clinical practice.

### 1.6.2 Intensity Modulated RadioTherapy

Intensity Modulated RadioTherapy (IMRT) represents a significant advancement over 3D CRT by taking better advantage of the MLC capabilities. Instead of delivering radiation with uniform intensity from each angle, IMRT dynamically adjusts the beam intensity to improve patient outcomes [38].

**Number of Beams** The choice of the number of beams in IMRT is a balance between treatment complexity and effectiveness. Using many beams can evenly spread the unwanted dose across all organs, but adds complexity to treatment planning and prolongs the delivery time, which can increase patient movement and reduce dose precision. Conversely, fewer beams simplify planning and shorten treatment time but may result in less optimal dose distribution. Research indicates that 50 beams are needed for "nearly optimal IMRT" [16]. Beams at exactly 180 degrees from each other tend to have (very) similar influence on the dose distribution on the patient. Therefore, dosimetrists tend to choose an odd number of equispaced beams. In practice, the number of beams used is below 25.

### 1.6.3 Volumetric Modulated Arc Therapy

Volumetric Modulated Arc Therapy (VMAT) enhances IMRT by allowing the MLC LINAC head to rotate while delivering radiation. Unlike IMRT, which stops the head at specific positions around the patient, VMAT continuously irradiates while rotating. This technique can better distribute the unwanted dose and reduces the irradiation time [18].

However, the mechanical constraints of the machine complicate the optimization problem for VMAT compared to IMRT, making the optimization more computationally intensive. Studies have demonstrated that, IMRT with a Sliding Window and more than 7 angles can achieve equally effective dose distribution [8] [45]. While demonstrated with IMRT Sliding Window, the techniques developed in this manuscript apply to VMAT, given sufficient computational resources.

## 1.7 Dosimetry steps

Dosimetry aims to design a treatment plan (i.e., machine instructions) that delivers the best possible dose for the patient. The "best" dose is difficult to define, so doctors formulate high-level clinical dose requirements. These requirements are abstract, so transitioning to machine instructions requires a series of sub-steps. For Intensity-Modulated Radiation Therapy (IMRT), three main steps are typically followed: Beam Orientation Optimization (BOO), Fluence Map Optimization (FMO), and Leaf Sequencing (LS).

### 1.7.1 Beams Orientation Optimization

Beam Orientation Optimization (BOO) is the initial dosimetry step. This step determines the optimal number of radiation beams and their respective angles. The beams' orientation significantly impacts the dose distribution within the patient: beams close to each other tend to have similar effects on the body. In contrast, far-apart beams tend to create doses impacting different tissues in the body. There is one exception to this rule of thumbs: Beams exactly 180° from each other can have a similar biological effect because rays will follow the same line, just entering the body from opposite directions. Despite its importance, the practical benefits of BOO are questionable. Research [47] suggests that an extensive BOO process offers only slight improvement over more straightforward strategies, like using equispaced beam angles. When using equispaced beams, it's common to use an odd number of beams to avoid beams at exactly 180° having the same effect. Employing an odd number of beams is standard practice when utilizing equispaced beam arrangements. This approach avoids beams positioned at precisely 180° from each other, with similar clinical effects (as mentioned before). Therefore, this manuscript will assume the use of an odd number of equispaced beams and no further BOO.

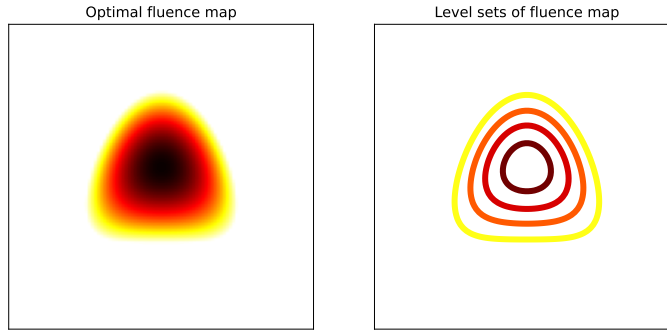


Figure 1.5: Example of a fluence map discretization.

### 1.7.2 Fluence Map Optimization

Fluence Map Optimization (FMO) is the critical step in the IMRT planning process. FMO aims to create fluence maps, i.e., a two-dimensional radiation intensity distribution on each beam's cross-sectional area. The fluence maps should be optimized to shape the dose distribution according to the treatment plan's objectives. At this stage, the physical constraints of the MLC still need to be considered; the primary focus is on achieving the desired dose distribution within the patient. The output of FMO is a set of idealized fluence maps for each beam.

### 1.7.3 Leaf Sequencing

Leaf Sequencing (LS) determines the specific positions and movements of the MLC leaves. The objective is to ensure that the delivered fluence map closely approximates the ideal fluence map generated during the Fluence Map Optimization (FMO) step. This approximation must be attained while considering the physical limitations of the treatment machine, such as irradiation power, leaf speed, or collimator speed, along with a soft constraint on the total treatment duration.

**Step and Shoot** The "Step and Shoot" technique in IMRT involves sequentially moving the MLC leaves to different positions to deliver varying radiation intensities. This technique for leaf sequencing is relatively simple computationally.

The fluence maps are divided into discrete levels (figure 1.5). Then, the MLC leaves are positioned so that the open area of the irradiation head matches the level set (figure 1.6). Note that convex level sets can all be matched with the MLC leaves; if the level set is concave, changing the collimator angle may allow the leaves to match the level set shape (figures 1.7a, 1.7b, 1.7c). Each level set is delivered as a static beam in sequence. As the level sets are refined, the irradiation time increases Dosimetrists must set a tradeoff between achieving greater accuracy and maintaining an efficient treatment time.

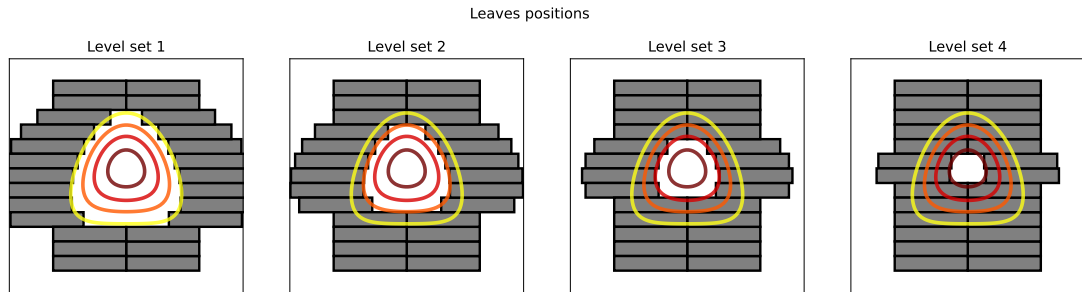
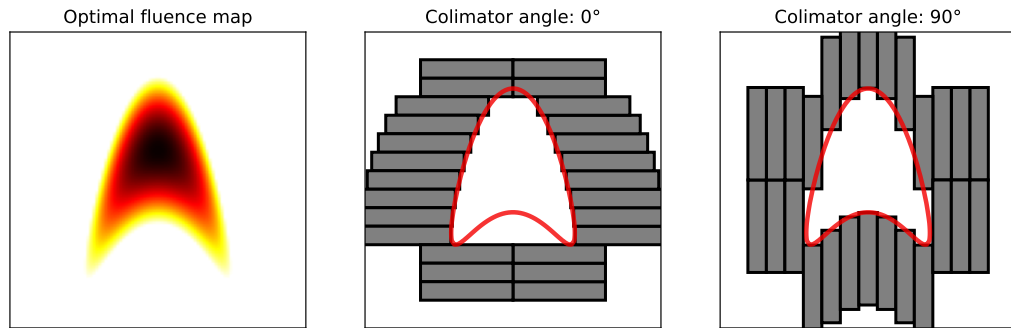
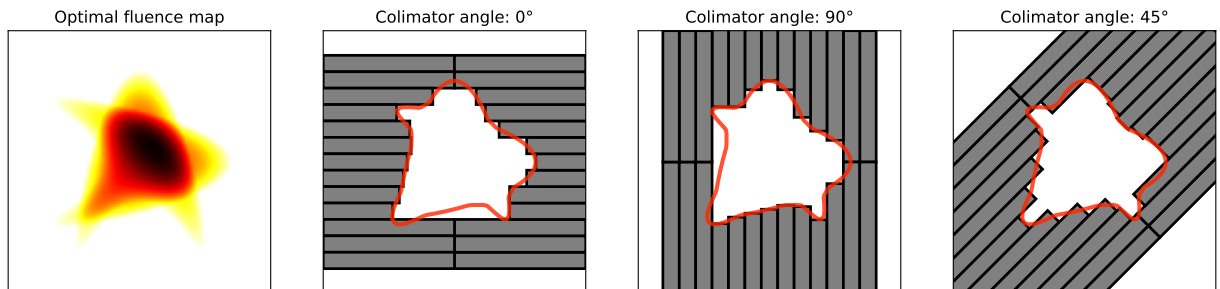


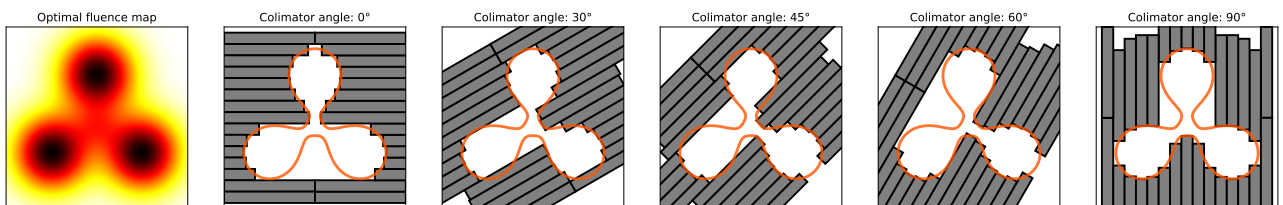
Figure 1.6: Example of level set matching with leaves.



(a) Example of a concave level set matched with leaves.



(b) Example of a more complex concave level set matched with leaves.



(c) Example of a concave level set impossible to match with leaves.

Figure 1.7: MLC leaves can not always be set to shape level sets of fluence functions.

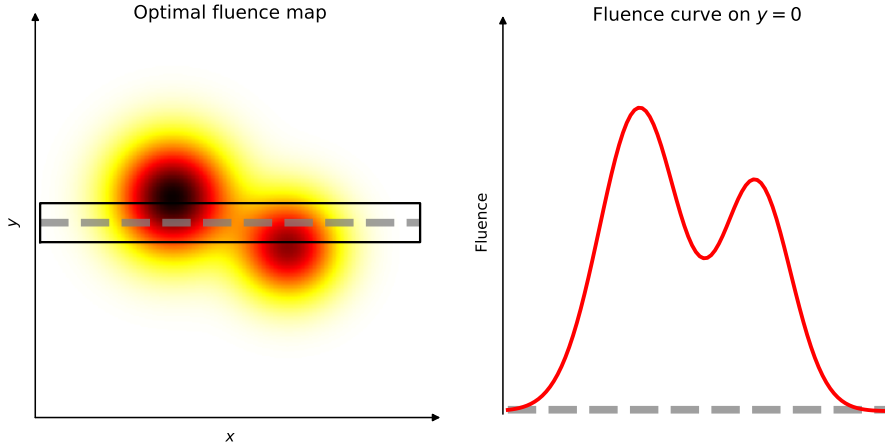


Figure 1.8: Example of a fluence map segmentation along a leaf pair axis.

**Sliding Window** The "Sliding Window" technique employs a continuous sweep motion of the MLC leaves. This approach enables the delivery of any continuous, positively defined fluence within the irradiation window of the MLC-LINAC. In contrast with step and shoot, a sliding window is more computationally intensive: Finding the appropriate leaf motions requires solving a linear programming problem for each pair of leaves (sometimes called "Inverse Sliding Window Algorithm").

The fluence is segmented in a one-dimensional fluence curve along each leaf pair axis (see figure 1.8). Suppose the motion of the leaves is from left to right: The difference between the time the right and left leaves pass by a point determines the amount of irradiation delivered at that point. The greater the time difference, the more rays will be sent from that point (in figure 1.9a and 1.9b, the time laps between left and right leaves passing a point is proportional to the fluence delivered at that point). One needs to carefully move the opening (right) and closing (left) leaves to deliver the correct amount of rays at each point of the fluence map. Solving a linear programming problem allows a leaf pair to deliver any fluence within arbitrary approximation in a reasonable amount of time (figure 1.9). A playground to calculate the leaf's motion for an arbitrary fluence is available here: <https://mics-lab.github.io/PresentationJuin2023PRFD/demo>.

The sliding window technique is used most of the time, as delivery time is much (about twice) faster [42]. This manuscript assumes the use of this technique, focusing on optimizing the fluence distribution.

#### 1.7.4 (Optional) Direct Aperture Optimization

Direct Aperture Optimization is mainly used in VMAT and occasionally employed to enhance IMRT plans. Unlike traditional approaches, which separate fluence map optimization from leaf sequencing, DAO directly optimizes the motion of the MLC leaves.

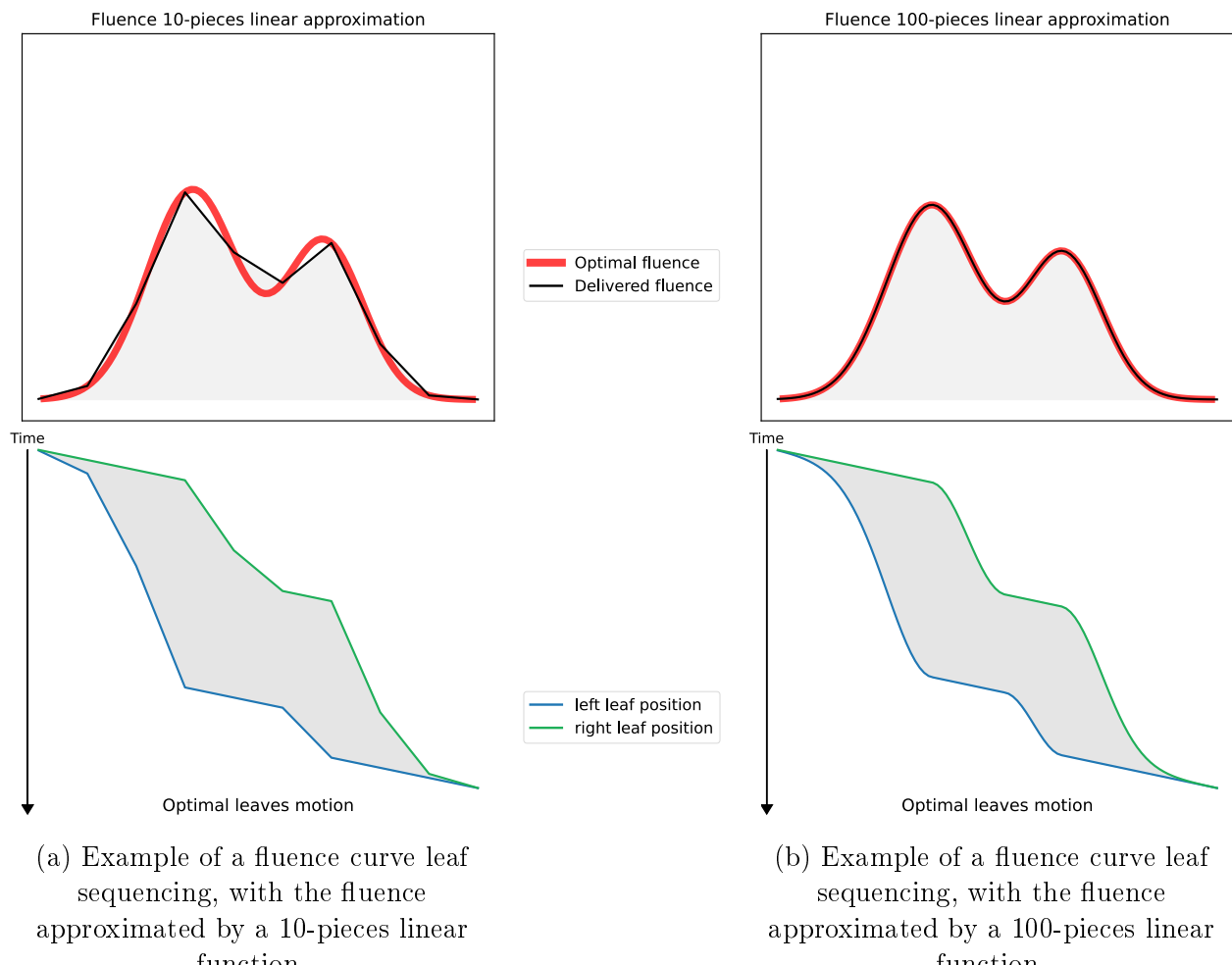


Figure 1.9: Fluence curve can be approximated with arbitrary error.

In VMAT, applying conventional leaf sequencing to any arbitrary fluence map is not feasible. Therefore, DAO is essential, as it is the only optimization method capable of generating a VMAT treatment plan.

When applied to IMRT, DAO can refine the treatment plan by directly adjusting the aperture shapes to better align with the desired dose distribution while accounting for the physical constraints of the treatment machine. However, as this manuscript is not focused on leaf sequencing, it assumes that no additional DAO is applied following conventional leaf sequencing.

## 1.8 Simulation

Throughout the dosimetry process, several approximations are employed. First, the assumption is that each bixel (beam pixel) operates independently. This approximation fails to account for interactions between adjacent bixels. Additionally, during FMO, ideal fluence maps are generated without considering the physical limitations of the treatment machine, such as the width of the multi-leaf collimator (MLC) leaves (often 5mm). Furthermore, the effects of beam penumbra and the scattering of radiation within the patient's body are often simplified or neglected in the FMO. Given these approximations, re-simulation of the treatment plan is critical to verify that the machine instructions deliver a dose distribution closely aligned with the expected outcomes.

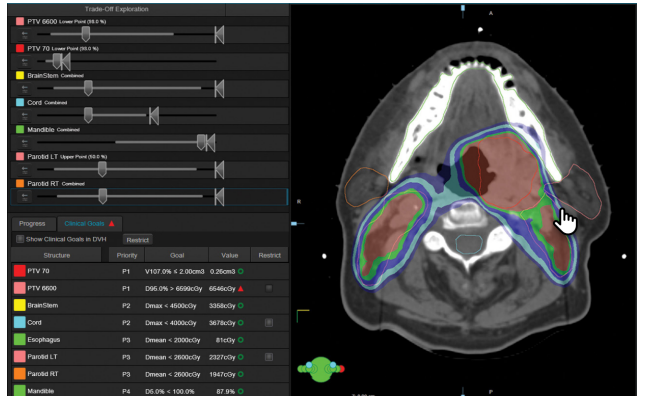
## 1.9 Treatment Planning Systems

Treatment Planning Systems (TPS) are the crucial tools that calculate the precise machine (MLC) motions according to the dosimetrists priorities and the irradiation technique chosen.

### 1.9.1 Manufacturer

#### Eclipse™ (Varian)

Eclipse™ [57], developed by Varian, is one of the most widely used TPS globally. It supports VMAT with one or multiple arcs, and IMRT with any number of beams. Eclipse™ integrates with Varian's suite of treatment machines, and integrates an automatic contouring tool [56].



Advertisement screenshot of Eclipse™ (Varian's TPS).

### ONE® | Planning (Elekta)

ONE® | Planning [14] is Elekta's TPS, and is also widely used, supporting IMRT and VMAT. It is renowned for its speed with high-precision dose calculation using the Monte Carlo method <sup>7</sup>.



Advertisement screenshot of  
ONE® | Planning (Elekta's TPS).

### Precision® (Accuray)

Developed by Accuray, Precision® [3] is the dedicated TPS for CyberKnife and TomoTherapy systems.



Advertisement screenshot of  
Precision® (Accuray's TPS).

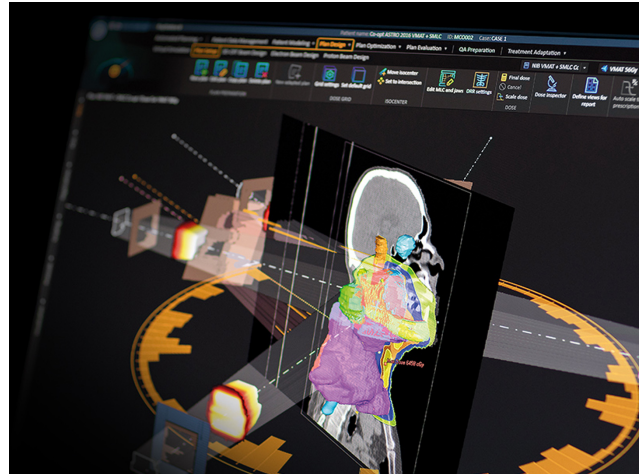
## 1.9.2 Non-manufacturer

---

<sup>7</sup>Monte Carlo methods are a class of computational algorithms that rely on repeated random sampling to obtain numerical results.

### **RayStation (RaySearch)**

RayStation [32], developed by RaySearch Laboratories, is a TPS known for its advanced optimization algorithms. Unlike manufacturer-specific systems, RayStation can output plans for a wide range of linear accelerators and imaging devices. It offers robust support for various treatment techniques, including VMAT, IMRT, 3D-CRT, Cyberknife, and TomoTherapy.



Advertisement screenshot of RayStation (RaySearch's TPS).

### **matRad (German Cancer Research Center - DKFZ)**

matRad [12] is an open-source TPS developed by the German Cancer Research Center (DKFZ) for research and education. While not intended for clinical use, matRad offers a flexible platform for testing and developing new treatment-planning algorithms.



### **AutoPlan (TheraPanacea - Unpublished)**

AutoPlan is the upcoming TPS from TheraPanacea, designed to incorporate artificial intelligence and machine learning into the treatment planning process.

# Introduction

## Abstract

Lorem ipsum dolor sit amet, consectetuer adipiscing elit. Ut purus elit, vestibulum ut, placerat ac, adipiscing vitae, felis. Curabitur dictum gravida mauris. Nam arcu libero, nonummy eget, consectetuer id, vulputate a, magna. Donec vehicula augue eu neque. Pellentesque habitant morbi tristique senectus et netus et malesuada fames ac turpis egestas. Mauris ut leo. Cras viverra metus rhoncus sem. Nulla et lectus vestibulum urna fringilla ultrices. Phasellus eu tellus sit amet tortor gravida placerat. Integer sapien est, iaculis in, pretium quis, viverra ac, nunc. Praesent eget sem vel leo ultrices bibendum. Aenean faucibus. Morbi dolor nulla, malesuada eu, pulvinar at, mollis ac, nulla. Curabitur auctor semper nulla. Donec varius orci eget risus. Duis nibh mi, congue eu, accumsan eleifend, sagittis quis, diam. Duis eget orci sit amet orci dignissim rutrum.

Nam dui ligula, fringilla a, euismod sodales, sollicitudin vel, wisi. Morbi auctor lorem non justo. Nam lacus libero, pretium at, lobortis vitae, ultricies et, tellus. Donec aliquet, tortor sed accumsan bibendum, erat ligula aliquet magna, vitae ornare odio metus a mi. Morbi ac orci et nisl hendrerit mollis. Suspendisse ut massa. Cras nec ante. Pellentesque a nulla. Cum sociis natoque penatibus et magnis dis parturient montes, nascetur ridiculus mus. Aliquam tincidunt urna. Nulla ullamcorper vestibulum turpis. Pellentesque cursus luctus mauris.

---

2.1	Context . . . . .	27
2.2	Problematic . . . . .	27
2.3	State of the Art . . . . .	27
2.4	Unsolved problems . . . . .	27
2.5	Contribution . . . . .	27

---

## 2.1 Context

Cancer; RT; optim to be done

## 2.2 Problematic

Manual optim is time consuming; need to automate

## 2.3 State of the Art

## 2.4 Unsolved problems

## 2.5 Contribution



# Dosimetry Optimization

## Abstract

Biological tissues are sensible to radiations in a non-linear manner [35], and slight variations in dose can have significant biological effects. Organs have differing sensibilities to radiation, which increases further the difficulty in formulating the goals to achieve when designing a radiation dose. Some organs can tolerate high cumulative doses if the radiation is well distributed. In contrast, others may withstand high doses at localized points ("hot spots") but cannot handle large doses overall. To address these differences, clinicians impose dose-volume histogram constraints in addition to the prescribed dose. Although the ideal objective is to minimize or eliminate radiation exposure to organs, achieving 0 Gy is impossible. The necessity of finding compromises drives the need for advanced optimization techniques to generate fluence maps that best satisfy the medical constraints. Therefore, various techniques can be used to calculate fluence maps (i.e., performing the critical fluence map optimization step). In this chapter, we explore some fluence map optimization techniques.

---

3.1	Discretization . . . . .	31
3.1.1	Bixels . . . . .	31
3.1.2	Voxels . . . . .	31
3.1.3	DI-Matrix . . . . .	31
3.2	Naive Optimization Method . . . . .	33
3.3	Constraints and Importance Factors . . . . .	34
3.3.1	Constraints Formulation . . . . .	34
3.3.2	Optimization Problem . . . . .	35
3.3.3	Balancing the Importance Factors . . . . .	39
3.4	Dose Mimicking . . . . .	40
3.5	Optimization Algorithm Review for Dosimetry . . . . .	40
3.5.1	Data . . . . .	40
3.5.2	Open-source Optimizers . . . . .	40
3.5.3	Results . . . . .	42
3.5.4	Discussion . . . . .	44

---

## 3.1 Discretization

The optimization process starts with transforming the continuous nature of both the radiation field and the human body into discrete elements. This transformation enables computation with modern computers.

### 3.1.1 Fluence Map Discretization: Bixels

Fluence maps are broken down into discrete elements called "bixels" (**b**eam **e**lements). Bixels represent small and independent beams of radiation (see a visualization figure 3.1).

The width of each bixel is constrained by the width of the multi-leaf collimator leaves. Modern multi-leaf collimator systems typically have a leaf width of 0.5 cm.

The height of a bixel can be selected arbitrarily, as the leaf can move continuously. Nevertheless, square bixels (akin to image pixels) are commonly used and will be employed throughout this manuscript.

It is essential to know that since negative energy rays are physically infeasible, we need to ensure that each bixel value is non-negative<sup>1</sup>. Bixels whose beams do not affect the planning target volume are typically excluded from calculations to improve computational efficiency. Activating these bixels could only degrade dose quality by increasing the dose to organs at risk without benefiting the dose distribution within the planning target volume.

### 3.1.2 Human Body Discretization: Voxels

The human body of the patient is also divided into discrete elements, as it is a three-dimensional object; the elements are "voxels" (**v**olume **e**lements). Each voxel represents a small portion of tissue within the patient's body, and will determine the granularity of the dose computed.

The maximum resolution of the voxel grid is defined by the planning image, which is typically a CT scan. It is common practice to resample the planning image to reduce computational demands. In this manuscript, where new techniques are explored, we have opted to resample the voxel grid to a resolution of 5 mm, ensuring a balance between computational efficiency and accuracy.

Additionally, to further optimize the computational process, only voxels corresponding to the planning target volume (PTV) and organs at risk (OARs) are retained for calculations. This selective approach reduces unnecessary computation.

### 3.1.3 Dose-Influence Matrix

The Dose-Influence Matrix (or DI-Matrix) links the discretized fluence map (the bixels values) and the discretized dose distribution within the patient (the dose on each voxel). This matrix

---

<sup>1</sup>In practice, to ensure positive bixel values, we use the absolute value element-wise.

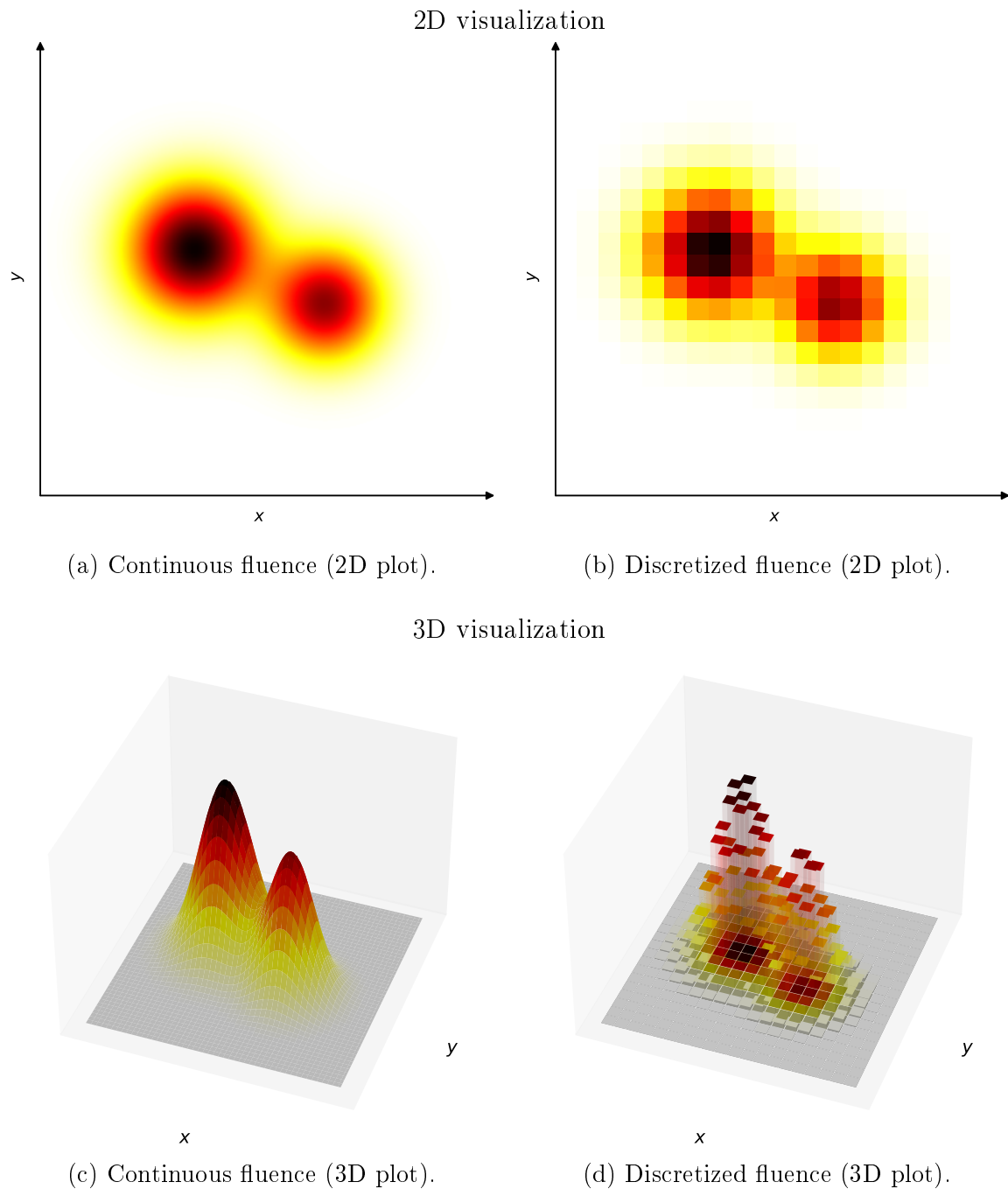


Figure 3.1: Example of a fluence discretized to  $20 \times 20$  bixels.

defines how the radiation from each individual bixel influences the dose delivered to every voxel in the patient's body.

We start by converting the 2D fluence map, composed of individual bixel values, into a column vector  $b$ . Similarly, we represent dose distribution in the patient's 3D space as a vector  $d$ , where each entry corresponds to the dose in a specific voxel. The DI-Matrix  $L$  governs the relationship between these vectors  $b$  and  $d$  via the matrix-vector multiplication  $d = Lb$ <sup>2</sup>. This mathematical operation computes the total dose at each voxel by summing the contributions from all active bixels (here, we assume that the effect of bixels is linear).

The DI-Matrix is constructed by simulating the radiation delivered by each individual bixel. For each bixel, the jaws of the multi-leaf collimator are virtually opened to allow only that specific beamlet to go through. A radiation transport model calculates the dose deposited in each voxel, considering the beam's spread and attenuation as it travels through the body. The resulting 3D dose deposition fills one column of the matrix  $L$ , corresponding to that bixel's influence on all voxels. Repeating this process for each bixel generates the entire DI-Matrix.

The accuracy of the dose calculation depends on the precision of the DI-Matrix. Simple models like pencil beam approximations, which assume a linear trajectory with minimal scattering, are considered too coarse. In contrast, more advanced simulations, such as Monte Carlo methods, provide a detailed and accurate dose calculation, although at a higher computational cost. In this manuscript, we employ collapsed cone convolution techniques (via TheraPanacea dose engine), which balance efficiency and accuracy.

## 3.2 Naive Optimization Method

A natural starting point in dose optimization is to attempt to directly achieve the delivery of a uniform dose, equal to the prescription, on all voxels within the PTV, and no dose elsewhere. We can attempt to find the bixels values delivering this dose by solving a least squares problem. We attempt to find the fluence map  $b$  that minimizes the difference between the actual dose  $d$  and the target dose  $d_{\text{target}}$ , which is set to the prescribed dose within the PTV.

Formally, the optimization problem can be stated as:

$$\min_b \|d_{\text{target}} - Lb\|^2, \quad b \geq 0$$

where  $d_{\text{target}}$  is the target dose vector, defined as follows for a prescription of  $p\text{Gy}$ :

$$d_{\text{target}} = p \cdot \mathbf{1}_{\text{PTV}}$$

Here,  $\mathbf{1}_{\text{PTV}}$  is the indicator vector for PTV that is equal to 1 for voxels within the PTV and 0 elsewhere.

---

<sup>2</sup>In practice, we compute  $d = L|b|$ , where  $|b|$  is absolute value of  $b$  element-wise to ensure positive bixel values.

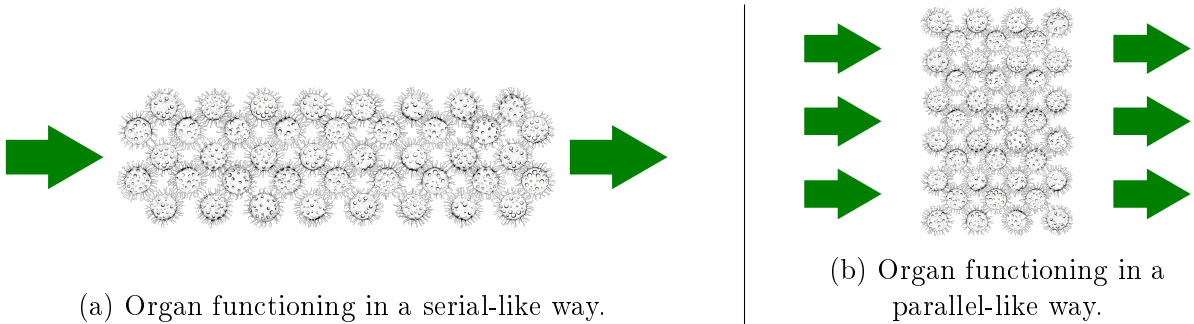


Figure 3.2: Organs functioning types.

To solve this problem, we perform a least squares minimization to find the optimal fluence map  $\mathbf{b}$ , where the matrix-vector multiplication  $\mathbf{L}\mathbf{b}$  yields the dose distribution  $\mathbf{d}$  across the entire patient volume.

However, this method is often inadequate in practice, as it attempts to solve the system based solely on the prescribed dose within the PTV, while neglecting any constraints on doses to the organs at risk (OARs). Since no constraints are imposed on the OAR doses, this naive optimization can result in high doses to critical structures, leading to unacceptable treatment plans. As a result, more sophisticated optimization methods that incorporate dose constraints on OARs and account for dose-volume constraints are necessary to achieve clinically viable treatment plans.

### 3.3 Constraints and Importance Factors

In order to obtain clinically acceptable doses, we need to incorporate the clinical aims in the optimization.

#### 3.3.1 Constraints Formulation

Different organs exhibit varying sensitivities to radiation, which influence their dose tolerance limits [?] [39]. Normal tissues are categorized as serial, parallel, or mixed, based on the functional organization of their sub-units. This classification determines the appropriate absorbed dose limits for normal tissues.

Serial organs (figure 3.2a), such as the spinal cord or esophagus, are characterized by a functional dependence on the integrity of every sub-unit. Damage to even a tiny region in these tissues can result in the loss of the organ's overall function. In contrast, parallel organs (figure 3.2b), such as the lung or liver, possess a reserve capacity where damage to a portion of the tissue does not necessarily impair overall function, as long as a critical volume remains intact.

We define two DVH value measures,  $V_X$  and  $D_{X\%}$ , for a structure  $S$ . For a given dose  $d : \mathbb{R}^3 \rightarrow \mathbb{R}^+$ ,  $V_X$  is defined as the volume of the three dimensional structure  $S \subseteq \mathbb{R}^3$  that receives a dose

equal to or higher than  $X$ , that is:

$$V_X = \frac{\text{Vol}(\{p \in S \subset \mathbb{R}^3 \mid d(p) \geq X\})}{\text{Vol}(S)}.$$

This formula can be approximated using the discretized dose on voxels  $\mathbf{d}$ :

$$V_X \approx \frac{\#\{v \in S \mid \mathbf{d}_v \geq X\}}{\#\{v \in S\}}$$

with  $v \in S$  voxels of the structure  $S$ ,  $\mathbf{d}_v$  the dose of  $\mathbf{d}$  associated with voxel  $v$ , and  $\#$  refers to voxel count.

Similarly, we define  $D_{X\%}$  as the minimal dose (in Gy) delivered to the  $X\%$  most irradiated region of the structure, that is:

$$D_{X\%} = \min \{d(p) \mid p \in S_{X\%}\}$$

where  $S_{X\%} \subseteq S$  is the  $X\%$  most irradiated region of  $S$ . Again, it can be approximated using the discretized dose on voxels  $\mathbf{d}$ :

$$D_{X\%} \approx \min \{\mathbf{d}_v \mid v \in S_{X\%}\}$$

where  $v \in S_{X\%}$  are the  $X\%$  most irradiated voxels of  $S$ .

For parallel-like structures, dose–volume reporting specifying  $V_D$  is commonly used, with  $D$  adapted to the specific organ. For instance, [24] demonstrated a correlation between the incidence and severity of lung pneumonitis and  $V_{20\text{ Gy}}$ , the volume of the lung receiving more than 20 Gy. In parallel-like structures, the median absorbed dose ( $D_{50\%}$ ) provides a valuable measure of the total dose delivered to the organ at risk.

For serial-like organs, it is recommended to report  $D_{2\%}$  as the maximum absorbed dose, as  $D_{0\%}$  is subject to noise.

Finally, for organs with a mixed parallel-serial structure, it is advised to report  $D_{50\%}$ ,  $D_{2\%}$ , and  $V_D$ , with  $D$  selected based on the threshold beyond which there is a significant risk of serious complications.

### 3.3.2 Optimization Problem

After the doctors have formulated maximal dose constraints for each OARs, and PTV coverage constraints  $\mathcal{C}$ , we can formulate the mathematical optimization problem.

Constraints  $c \in \mathcal{C}$  are formulated as  $c = (S, D, V, \pm)$  where  $D$  is in Grey,  $V$  is a %, and  $\pm$  means the constraint is maximal/minimal.

**E.g.:**  $c_{PTV+} = (\text{PTV}, 76\text{ Gy}, 95\%, +)$  means that for the PTV structure, we need  $D_{95\%} \geq 76\text{ Gy}$  (or, equivalently,  $V_{76\text{ Gy}} \geq 95\%$ ); this is a very typical constraint [63].

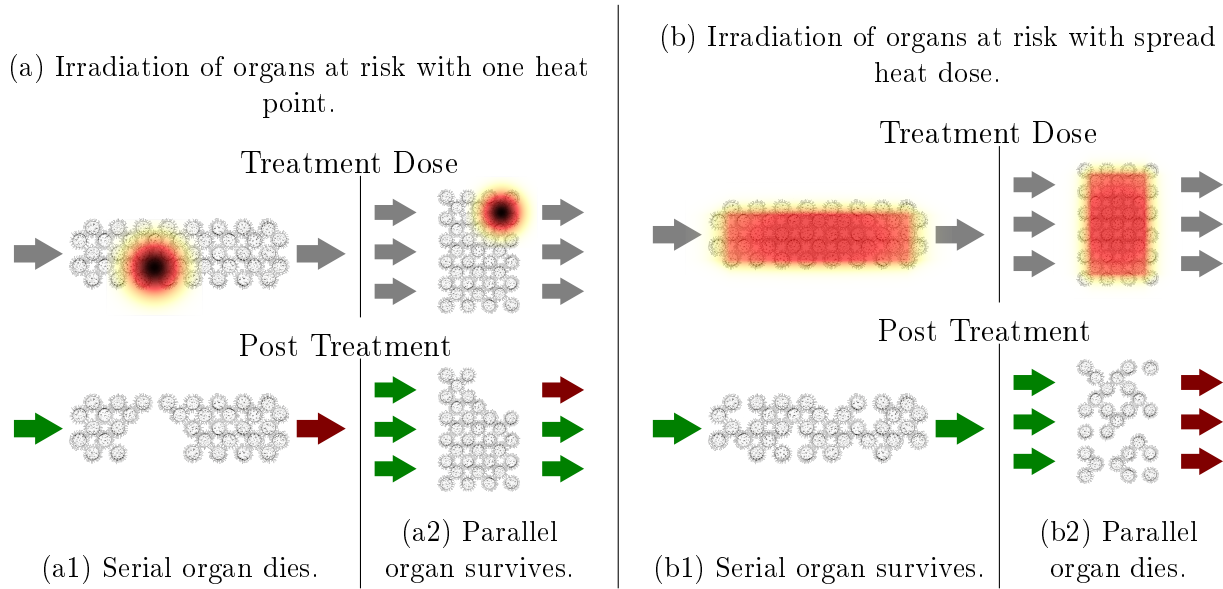
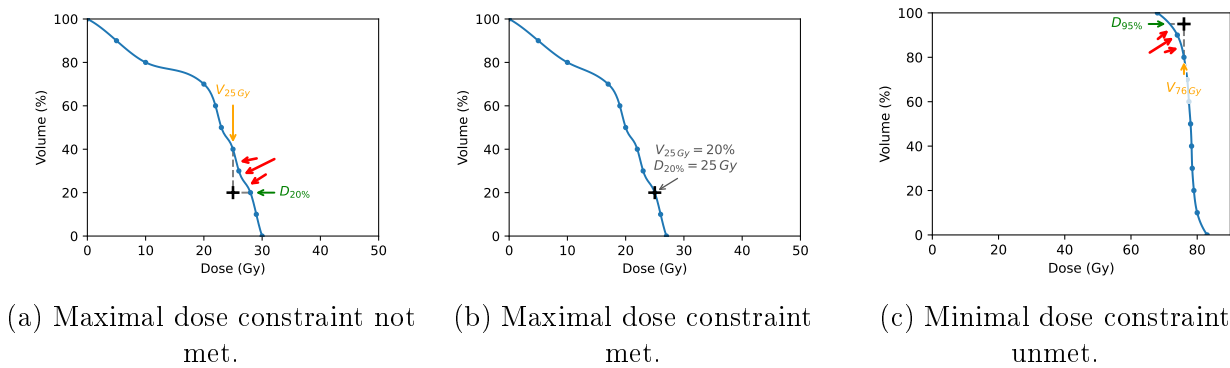


Figure 3.3: Irradiation type survival of organs serial-like and parallel-like.



Figures 3.4a, 3.4b: Typical DVH of an OAR, with visualization of the maximal dose constraint  $D_{20\%} \leq 25 \text{ Gy}$  (or  $V_{25\text{Gy}} \leq 20\%$ ).

Figure 3.4c: Typical DVH of a PTV, with visualization of the minimal dose constraint  $D_{95\%} \geq 76 \text{ Gy}$  (or  $V_{76\text{Gy}} \geq 95\%$ ).

Note that dose-volume objectives then turn to points on dose-volume histograms. The relevant DVH curve must stay above (in the case of a minimal dose constraint), or under (in the case of a maximal dose constraint) this point to pass the constraint.

**E.g. (bis):**  $c_{\text{organ}} = (\text{organ}, 25 \text{ Gy}, 20\%, -)$  means that for the 'organ' structure, we need  $D_{20\%} \leq 25 \text{ Gy}$  (or, equivalently,  $V_{25 \text{ Gy}} \leq 20\%$ ). This constraint example is illustrated in figure 3.4a, 3.4b, 3.4c.

We only calculate a voxel-discretized version  $\mathbf{d}$  of the dose  $d : \mathbb{R}^3 \rightarrow \mathbb{R}^+$ , using a bixel-discretized version  $\mathbf{b}$  of the fluence maps  $f^\theta : \mathbb{R}^2 \rightarrow \mathbb{R}^+$  for each selected angle  $\theta$ . Hence, we formulate the optimization problem on the discretized information.

**Ideal Case** In the ideal case, it is possible to meet all constraints, and we try to minimize further the dose  $\mathbf{d}$  on the OARs. Mathematically, we find the values for  $\mathbf{b}$  giving dose  $\mathbf{d} = \mathbf{Lb}$  such that all DVH constraints  $\mathcal{C}$  are satisfied, and  $\sum_{v \in \text{OARs}} \mathbf{d}_v^2$  is minimum (where  $\mathbf{d}_v$  is the dose on voxel  $v$ , and  $v \in \text{OARs}$  are the voxels  $v$  belonging to an OAR):

$$\min_{\mathbf{b}} \sum_{v \in \text{OARs}} \mathbf{d}_v^2 \quad \text{with } \mathbf{d} = \mathbf{Lb}, \mathbf{b} \geq 0 \text{ and such that } \forall c \in \mathcal{C}, c \text{ is satisfied.}$$

**Practical Case** In practice, constraints formulated by the doctors are too hard to satisfy. Hence, we create one objective function  $f_c$  for each constraint  $c \in \mathcal{C}$ , which decrease as we get closer to satisfying the constraint. The optimization problem becomes:

$$\min_{\mathbf{b}} \sum_{c \in \mathcal{C}} w_c f_c(\mathbf{d}) \quad \text{with } \mathbf{d} = \mathbf{Lb}, \mathbf{b} \geq 0$$

with  $w_c$  importance factor of constraint  $c$ .

**Penalization functions** Given a constraint  $c = (S, D \text{ Gy}, V\%, \pm)$ , multiple approaches can be considered for defining an objective function  $f_c$ . Here, we explore three commonly used methods (also visually explained in figure 3.5):

1. **Penalizing the lower  $100 - V\%$  dose voxels:** This method penalizes a fixed number of voxels but tends to be noisy since the lower  $V\%$  voxels can fluctuate with each optimization iteration.
2. **Penalizing voxels with dose  $> D \text{ Gy}$ :** This approach yields a convex objective function.
3. **Penalizing the lower  $100 - V\%$  dose voxels with dose  $> D \text{ Gy}$ :** This method is the most advanced method; Note that once the constraint is satisfied, no voxel is penalized. However, for the same reason as the first approach, this penalization remains prone to noise.

Turning off penalization is possible once a constraint is met (this is useful for the first two methods presented above). In our implementation, we chose not to do so, so when a constraint is on the edge of being met, the penalization does not turn on and off every other optimization iteration.

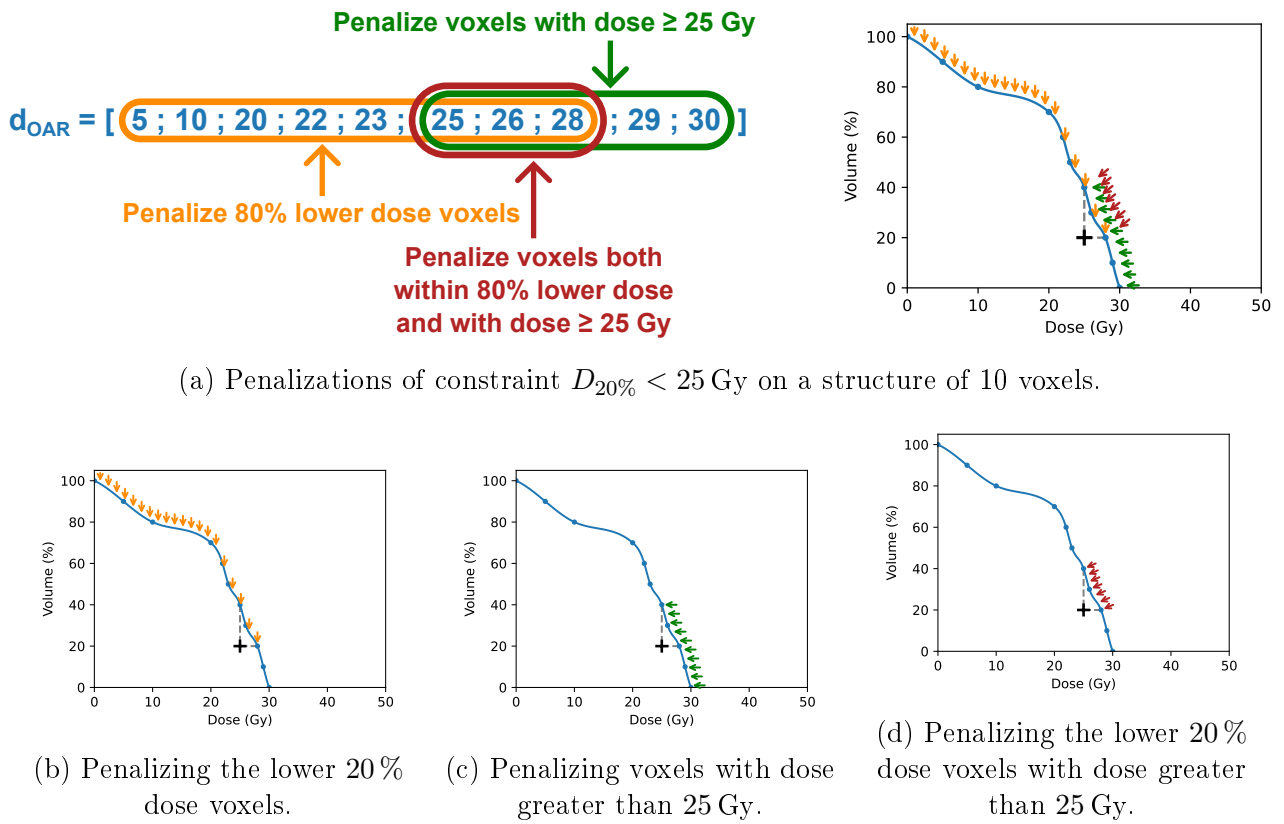


Figure 3.5: Typical penalization of a dose on an OAR according to the maximal dose constraint  $D_{20\%} \leq 25 \text{ Gy}$ .

Once the set of penalized voxels is selected, the penalization power  $p$  must be determined, with typical choices being  $p = 1$  or  $p = 2$ . We opt for penalizing voxels with a dose greater than  $D$  Gy and set  $p = 2$ . This choice makes the objective function convex a weighted sum of convex functions. Desirable properties, such as the existence of a unique global minimum once the values of  $w_c$  are fixed, follow from the convexity of the objective function.

Finally, the mathematical formulation of the objective function associated with the constraint  $c = (S, D, V, \pm)$  is:

$$f_c(\mathbf{d}) = \sum_{v \in S} (\mathbf{d}_v - D)_+^2$$

and the global minimization problem becomes

$$\min_{\mathbf{b}} \sum_{c \in C} w_c \sum_{v \in S} (\mathbf{d}_v - D)_+^2 \quad \text{with } \mathbf{d} = \mathbf{L}\mathbf{b}, \mathbf{b} \geq 0$$

where  $w_c$ , the weights or importance factors of each constraint, are to be determined.

**Bixel regularization** For optimal leaf sequencing, it is preferable to have smooth bixel values, meaning that adjacent bixels should have minimal variation in their values. A regularization term was incorporated to achieve this, penalizing discrepancies in bixel values relative to their neighboring bixels using a squared penalty function.

### 3.3.3 Balancing the Importance Factors

The importance factors  $w_c$  play a crucial role in the optimization process. These weights allow dosimetrists to prioritize certain clinical constraints over others. Properly balancing these factors ensures that the most critical aspects of the treatment plan are emphasized while still striving to meet all constraints.

The constraints associated with the PTV, ensuring the destruction of the tumor, conflict with the protection of the OARs. Hence, the optimization process becomes a trade-off between satisfying different constraints. For example, increasing the dose of the PTV will inadvertently increase the dose of nearby OARs. Carefully tuning of the importance factors ensures that the optimization algorithm directs the fluence maps towards a solution that balances the therapeutic benefits with the risk of complications.

Due to the unique geometry of each patient, an optimal dose plan cannot be applied universally. The optimization must be recalculated for every patient. Dosimetrists customize the dose to meet the specific needs of each individual patient by taking into account clinical priorities, spatial relationships, and physician expertise. This process is time consuming, and remains manual; this manuscript tackles the problem of treatment planning.

The contouring task used to be a manual operation but is now done automatically, thanks to the progress of artificial intelligence on segmentation tasks [29] [13]. After the emergence of AI for contouring, this manuscript tackles the problem of automatic treatment planning.

## 3.4 Dose Mimicking

Dose mimicking is a technique used to reproduce a dose distribution as closely as possible. It involves the optimization of a new treatment plan to match the dose profile of an existing plan, which is typically derived from either a prior treatment or a reference plan considered clinically acceptable. This differ from the naive approach in 3.2: the dose distribution that we try to replicate is not manually set. The target dose was achieved before either on the same machine, or on a similar MLC. Hence, the task of mimicking it should be "easier".

Formally, the optimization problem can be stated the same way as in 3.2:

$$\min_{\mathbf{b}} \|\mathbf{d}_{\text{target}} - \mathbf{L}\mathbf{b}\|^2$$

with  $\mathbf{d}_{\text{target}}$  the previously target dose, instead of the manually defined one.

## 3.5 Optimization Algorithm Review for Dosimetry

The selection of an optimization algorithm is critical. Different algorithms may converge to various local minima when dealing with non-convex objective functions, potentially leading to significant outcome variations. To mitigate this issue, we have designed the objective function to be convex, ensuring all optimization methods converge to the same global minimum. In this study, we benchmark the computational complexity and convergence rates of various algorithms. These findings are intended to provide valuable insights for the development of TPS.

### 3.5.1 Data

We focused on evaluating the various open-source optimizers. We used the widely recognized TG-119 [40] cases as a benchmark for evaluating radiation therapy plan optimization. The TG-119 dataset provides specific dose goals, which we incorporated into our proposed cost function. The TGG 119 multiple PTVs is a theoretical case unlikely to happen in real life. However, the other cases represent a comprehensive set of what dosimetrists could encounter daily.

We also used one typical case of prostate cancer from ICM. For this case, doctors had provided specific dose goals that we again incorporated into our proposed cost function.

### 3.5.2 Open-source Optimizers

We tried to have a comprehensive set of available open-source optimizers.

**(Stochastic) Gradient Descent** Is an optimization algorithm that iteratively updates the model parameters in the direction of the negative gradient of the objective function. In our case, it is not stochastic since it calculates the gradient using the current solution<sup>3</sup> [22].

---

<sup>3</sup>Our objective function has all its inputs as parameters, so there is no notion of stochasticity.

**Conjugate Gradient** Is an iterative optimization algorithm commonly used to solve systems of linear equations or quadratic optimization problems. It iteratively computes conjugate directions and updates the solution along them, aiming to minimize the objective function [20]. Conjugate Gradient is often applied in scenarios where the Hessian matrix is unavailable or computationally expensive.

**Newton** Newton's method is an iterative optimization algorithm that uses the second-order derivative (Hessian matrix) to find the minimum of a function. It updates the current estimate by considering both the first-order derivative (gradient) and the second-order derivative [43].

**SLSQP** (Sequential Least Squares Programming) is a sequential quadratic programming algorithm for constrained optimization. It iteratively solves a sequence of quadratic programming subproblems to find the optimal solution subject to constraints [7].

**RMSprop** (Root Mean Square Propagation) is an optimization algorithm that addresses the problem of diminishing learning rates in traditional gradient descent methods. It divides the learning rate by the root mean square of the past gradients, which helps to stabilize and speed up convergence [21].

### BFGS-based

**Pure BFGS** (Broyden-Fletcher-Goldfarb-Shanno) is a quasi-Newton method that approximates the Hessian matrix using updates based on gradient information. It performs a line search to determine the step size that minimizes the objective function along the search direction [17].

**L-BFGS** (Limited-memory BFGS) is a variation of BFGS that uses a limited-memory approach to approximate the Hessian matrix. It stores a limited number of past gradient and parameter values to compute an approximate inverse Hessian matrix efficiently [33].

### Adam-based

**Pure Adam** (Adaptive Moment Estimation) is an optimization algorithm combining ideas from adaptive learning rates and momentum methods. It computes adaptive learning rates for each parameter based on estimates of the first and second moments of the gradients [30].

**RAdam** (Rectified Adam) is a variant of the Adam optimizer that introduces a rectification term to stabilize the adaptive learning rate. It aims to address some convergence issues that may occur in Adam by dynamically adjusting the variance of the adaptive learning rate [34].

**NAdam** (Nesterov Adam) combines the Nesterov accelerated gradient method with the Adam optimizer. It incorporates Nesterov momentum into the Adam update rule to improve convergence and provide better generalization [53].

**AdamDelta** Is another variant of the Adam optimizer that replaces the second moment estimates (variance) with a delta parameter. It eliminates the need for storing and updating the moving average of the squared gradients, which can be beneficial in memory-constrained settings [62].

**Adamax** Is an extension of the Adam optimizer that uses the gradients' infinity norm (max norm) instead of the L2 norm. It is designed to handle sparse gradients more effectively and can be particularly useful in deep learning models [6].

**Rprop** (Resilient Backpropagation) is an optimization algorithm specifically designed for neural networks. It adaptively updates the weights based on the gradient sign, adjusting the step size. Rprop performs weight updates independently for each weight parameter [46].

**Other optimizers variations** In addition, we tested AdamW, Adagrad, and ASGD. However, AdamW and Adagrad behaved similarly to Adam, and ASGD behaved similarly to SGD. For readability purposes, we did not include them in the results plots.

### 3.5.3 Results

**Newton's method** Based on the iterations-wise graph analysis, Newton's method performs best, consistently achieving a stable converged state within ten steps across all four examined cases. However, Newton's method steps are computationally expensive since it uses a second-order derivative (the Hessian) that is difficult to compute.

It is widely recognized that Newton's method excels in optimizing convex functions [44]. Our objective function is convex by construction; hence, this optimization algorithm is particularly effective.

**LBFGS vs BFGS** It would be expected that BFGS performs better than LBFGS in terms of iterations but not in terms of time (since LBFGS is a fast approximation of the BFGS technique). However, we observe that LBFGS outperforms BFGS even on the iterations-wise graph. This performance suggests that the limited memory approximation is biased towards suitable directions in these problems.

**Best Algorithms** Besides Newton's method, three algorithms have similar performances: Adam, Adamax, and LBFGS. Adam and Adamax appear to have more "wavy" cost curves, while LBFGS cost decreases more stably. These observations are valid both in terms of iteration and time.

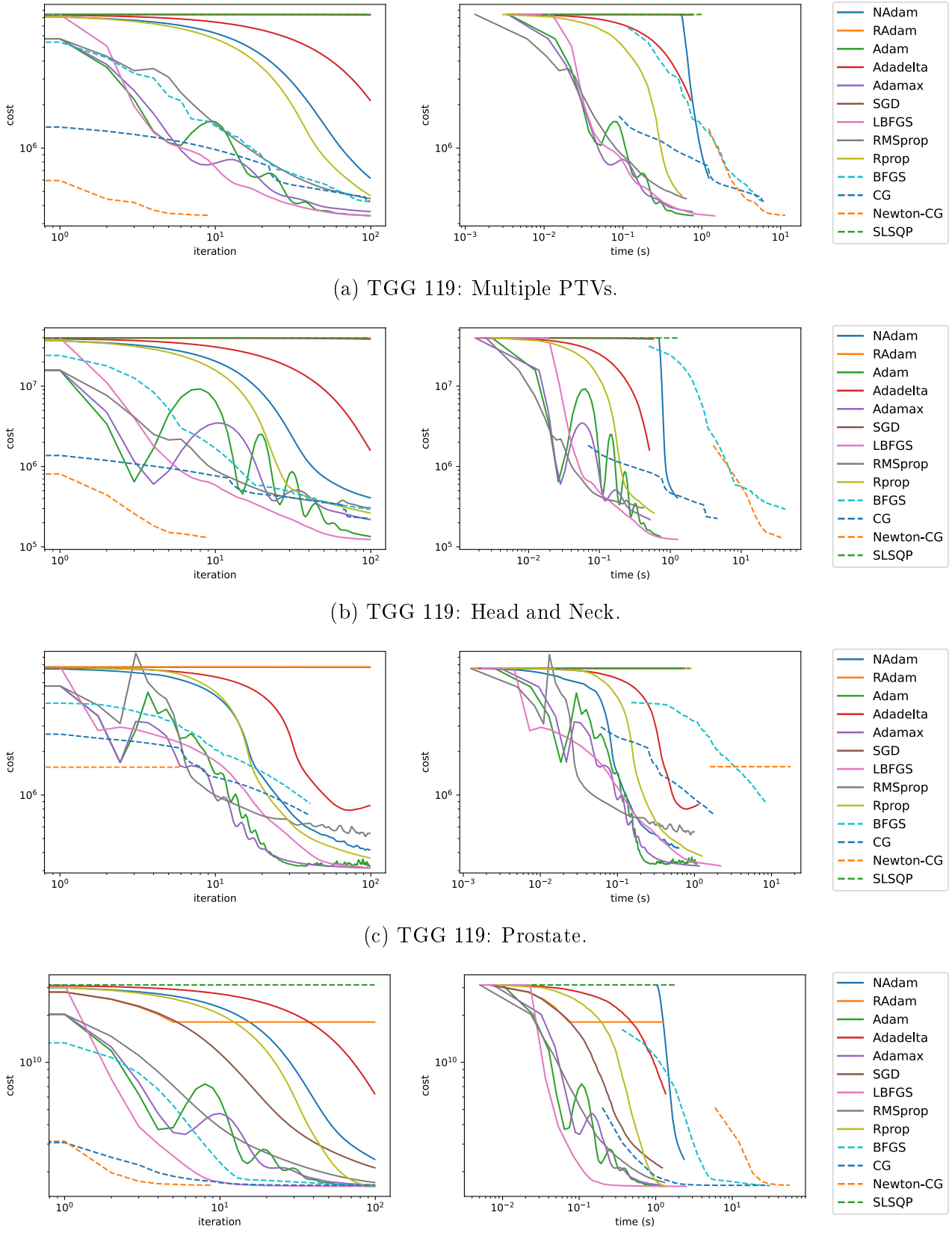


Figure 3.6: Evolution of the objective function value ('cost') through optimization iterations and computation time for four typical dosimetry cases.

TGG 119 Multiple PTVs (figure 3.6a) is the smallest problem, and the real ICM prostate case (figure 3.6d) is the largest problem (in terms of patient/organs/structure volume size); TGG 119 fake head and neck (figure 3.6b) and TGG 119 fake prostate (figure 3.6c) have similar sizes. Notably, an observable trend indicates that as the problem size increases, LBFGS outperforms both Adamax and Adam optimization algorithms.

Therefore, we will use the LBFGS algorithm in the rest of this manuscript.

### **3.5.4 Discussion**

In the future, if new techniques are developed one day, making computing the Hessian much faster, we recommend using Newton's optimization algorithm. However, to our knowledge, computing the Hessian remains long, not only in our implementation.

Hence, we recommend using the LBFGS algorithm for the problem of dose optimization in radiotherapy; it is the fastest to converge and converges steadily on the tested cases.

# Doses Relationship

## Abstract

Fluence Map Optimization (FMO) requires selecting importance factors for each clinical constraint, which reflect the relative priority of achieving specific dose goals. These importance factors significantly influence the resulting dose distribution, as varying their values can lead to diverse treatment outcomes. This chapter investigates the relationship between the chosen importance factors and the resulting dose distributions. We aim to understand how different configurations affect the trade-offs between conflicting clinical objectives. This analysis provides insight into optimizing importance factors to achieve the most clinically effective treatment plans.

---

4.1	Distance Between Doses . . . . .	47
4.1.1	Method . . . . .	47
4.1.2	Results . . . . .	54
4.1.3	Discussion . . . . .	57
4.2	Network of Doses . . . . .	58
4.2.1	Introduction . . . . .	58
4.2.2	Radiotherapy . . . . .	58
4.2.3	Methods . . . . .	58
4.2.4	Results . . . . .	59
4.2.5	Discussion . . . . .	59
4.2.6	Conclusion . . . . .	59
4.3	Novel Dosimetry Automation Approach with Graph Theory . . . . .	59

---

## 4.1 Distance Between Doses

In this section, we aim to establish a robust metric for quantifying the distance between different dose distributions. Such a distance should provide a numerical comparison that reflects the clinical discrepancies between two dose distributions. By developing a distance measure that captures these nuances, we can better evaluate and compare treatment plans.

**A non-trivial task** Quantifying the difference between two dose distributions, particularly regarding clinical impact, is inherently challenging. This complexity arises because not all patient anatomy regions contribute equally to treatment outcomes. Dose variations in critical structures may significantly influence clinical effects, while similar variations in less critical areas may have negligible impact. Moreover, the potential for dose compensation (underdosing in one region counterbalancing overdosing in another) further complicates the development of a reliable metric for comparing dose distributions. This compensatory effect is only sometimes applicable, making establishing a standardized method for assessing dose distribution clinical differences challenging.

**Dose Evaluation** To assess the quality of a dose distribution, dosimetrists primarily focus on DVHs as the key metric. While they also consider aspects of the three-dimensional (3D) dose distribution, such as inter-structure dose gradients and the presence, number, and location of hot spots, their primary attention is directed towards the analysis of DVHs, which provide a comprehensive overview of dose coverage and sparing of organs at risk.

### 4.1.1 Method

**Naive Doses Comparison** The most straightforward method for comparing two dose distributions, thus defining a distance metric, is to perform a voxel-by-voxel comparison of the dose values. However, this approach overlooks the inherent anatomical structure of the human body and the fact that not all voxels have the same clinical significance. Consequently, even if the voxel-wise distance between two dose distributions is considerable, their overall clinical effects may still be similar.

**Pathological example** We constructed a simplified example, as illustrated in Figure 4.1. This hypothetical scenario involves a phantom model consisting of a homogeneous water-equivalent material containing a cubic planning target volume (PTV) and a cubic organ-at-risk (OAR). Although this model lacks anatomical realism, it effectively highlights the limitations of using basic voxel-wise comparisons for dose evaluation. It emphasizes the need for more sophisticated techniques to capture clinically relevant differences in dose distributions accurately.

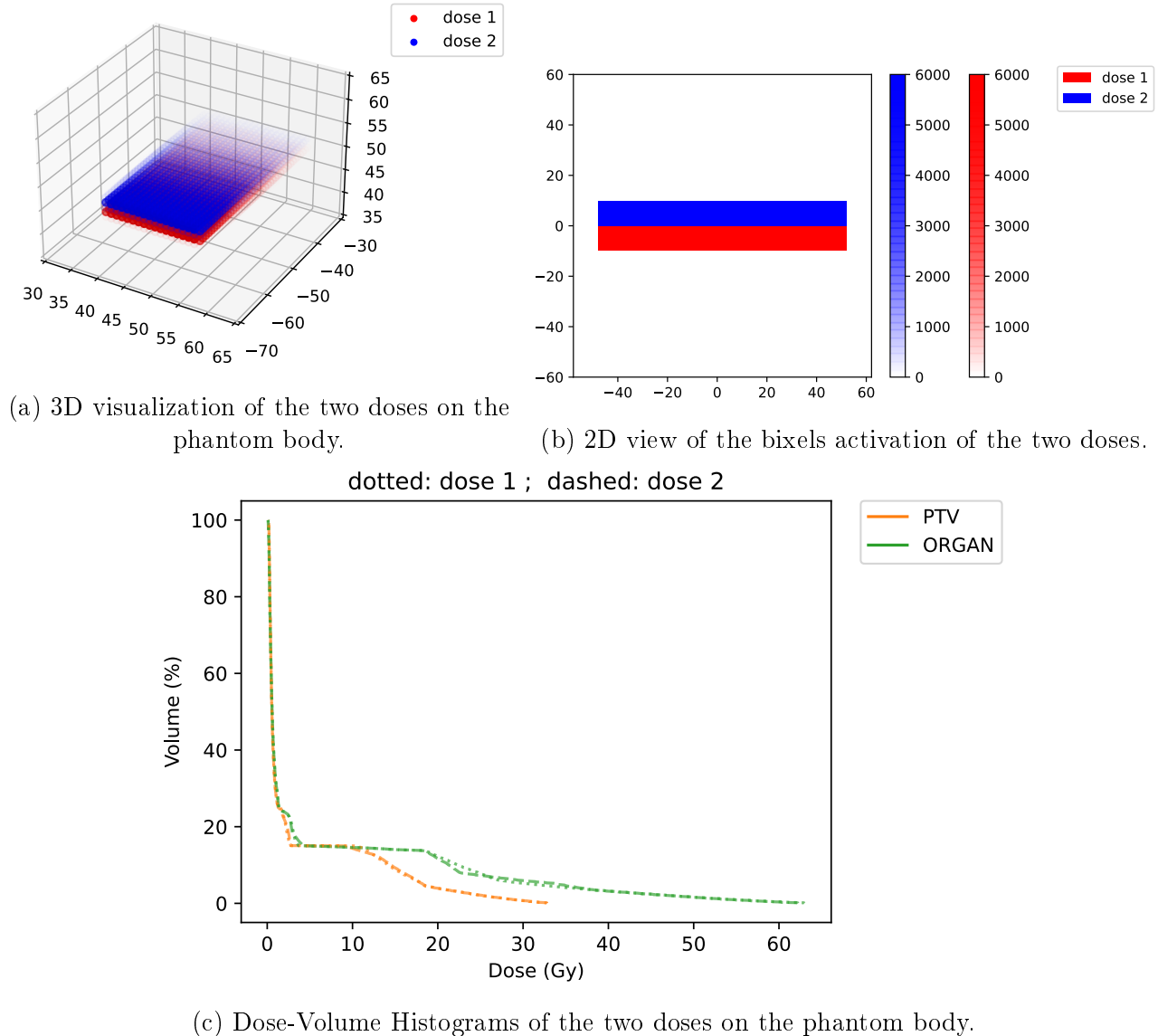


Figure 4.1: Example of two doses that have the same clinical effect (measured from the DVHs), but very different voxel-wise dose values.

### 4.1.1.1 Doses Samples

We assessed the efficacy of our proposed method for comparing radiation doses using the TG-119 Prostate case, a well-established benchmark for evaluating radiation therapy plans [40]. The TG-119 dataset includes predefined dose objectives, which we utilized to formulate our cost function. We performed optimizations with different weight assignments applied to each constraint to generate varying treatment dose distributions for the same patient case under identical constraints.

### 4.1.1.2 Distances Between Doses

**Comparing Doses Voxel-wise** When two radiation dose distributions are closely aligned, the voxel-wise comparison is an effective measure, as it can be assumed that the global distribution is similar. This approach allows for a detailed comparison of local dose variations. Mathematically, given the voxel-wise dose  $\mathbf{d}$ , the distance between two dose distributions,  $\mathbf{d}^1$  and  $\mathbf{d}^2$ , is defined as the norm of their difference:  $\sum_{v \in \mathcal{V}} |\mathbf{d}_v^1 - \mathbf{d}_v^2|$ , where  $v$  represents the voxels in the set of interest  $\mathcal{V}$ , and  $\mathbf{d}_v^i$  is the dose value at voxel  $v$  for dose distribution  $\mathbf{d}^i$ <sup>1</sup>. However, voxel-wise distance can become misleading if two regions of equal volume within the same anatomical structure have their dose values swapped. In such cases, the voxel-wise difference would appear large despite the clinical equivalence of the two doses. Furthermore, this method is limited to comparing doses within the same patient, as it requires a direct correspondence between the dose voxels in both distributions.

**Comparing Dose Volume Histogram Curves** We propose comparing the Dose Volume Histogram (DVH) curves. We have one curve for each structure; we define the distances between doses for each structure, and in the end, we sum up all structures to end up with a single scalar distance between two doses. We can quantify the variation between the two dose distributions in aggregated forms, using the structures.

**Discrete DVH Approximation** The DVH is obtained after sorting the voxel-wise dose of the structure: Let  $\mathbf{d}[s]$  be the voxel-wise dose of the structure  $s$  (therefore, a list, of length  $n[s]$ , the number of voxels that belong to the structure). Let  $\hat{\mathbf{d}}[s]$  be the list above in descending order (i.e.  $\hat{\mathbf{d}}[s]_i > \hat{\mathbf{d}}[s]_j$  if  $0 < i < j \leq n[s]$ ). Then, the DVH of  $s$  can be approximated by the continuous line composed of the segments linking the following points:  $(\hat{\mathbf{d}}[s]_i, i/n[s])$   $0 < i \leq n[s]$ . Since we compute the dose voxel-wise, we may only have an approximation of the DVH. However, in practice, most structures of interest have more than a hundred voxels, which makes the DVH approximation very precise.

Since we draw one curve per structure of interest, this capture some of the importance of voxel over others. In fact, when analyzing a dose, doctors look at the dose volume (voxel-wise),

---

<sup>1</sup>This is often written as  $|\mathbf{d}_1 - \mathbf{d}_2|$ , with the summation over voxels implied.

but they also take a close look at the DVHs; this is an incentive that DVHs should contain meaningful information.

**Distance Measure** To measure how different two DVH curves, we can imagine several techniques:

- Fréchet distance (treating DVHs as curves in a 2D space)
- Hausdorff distance (treating DVHs as 1D manifolds in a 2D space)
- Wasserstein distance (treating DVHs as probability distributions)
- Kolmogorov-Smirnov test (treating DVHs as probability distributions)
- Total variation between curves (treating DVHs as functions)

We evaluated all the aforementioned distance metrics and propose to retain only the one that yields the most clinically meaningful results.

**Fréchet Distance** DVH (Dose-Volume Histogram) curves can be interpreted as lines in R2R2<sup>2</sup>. In this context, the Fréchet distance is a well-known metric for assessing the similarity between two curves, particularly useful for comparing poly-lines [?]. It measures the minimum distance a particle would travel when simultaneously traversing both curves. In this study, we apply the Fréchet distance to compare the DVH curves of two radiation dose distributions.

Formally, let  $P$  and  $Q$  represent the curves being compared, with  $\gamma$  denoting a parametrization defined on the interval  $[0, 1]$ . The positions of a particle moving along curves  $P$  and  $Q$  at time  $t$  are given by  $P(\gamma(t))$  and  $Q(\gamma(t))$ , respectively. The Fréchet distance is defined as:

$$d_{\text{Fréchet}}(P, Q) = \inf_{\gamma} \max_{t \in [0, 1]} d(P(\gamma(t)), Q(\gamma(t)))$$

When applied to DVH curves, let  $\mathcal{C}_A$  and  $\mathcal{C}_B$  denote the discrete DVH curves of two dose distributions. These curves consist of line segments connecting a series of points  $\{\mathcal{C}_A(i) = (d_i, v_i), 1 \leq i \leq n_A\}$  and  $\{\mathcal{C}_B(j) = (\tilde{d}_j, \tilde{v}_j), 1 \leq j \leq n_B\}$ ; where  $d_i$  and  $\tilde{d}_j$  denote the dose levels<sup>3</sup>,  $v_i$  and  $\tilde{v}_j$  represent the corresponding volumes, and  $n_A$  and  $n_B$  are the number of points forming  $\mathcal{C}_A$  and  $\mathcal{C}_B$ <sup>4</sup>.

The Fréchet distance, in this case, is defined as the infimum over all possible traversal times. Given that the curves are discrete line segments, the Fréchet distance can be expressed as:

$$d_{\text{Fréchet}}(\mathcal{C}_A, \mathcal{C}_B) = \min_{\substack{j: \llbracket 1, n_A \rrbracket \rightarrow \llbracket 1, n_B \rrbracket \\ j \nearrow (j \text{ increasing})}} \sum_{i=1}^{n_A} dist(\mathcal{C}_A(i), \mathcal{C}_B(j(i)))$$

---

<sup>2</sup>In the case of voxel-wise dose approximations, they are represented as poly-lines in R2R2.

<sup>3</sup>Derived from  $\mathbf{d}$  after selecting voxels of the structure of interest, and sorting voxels.

<sup>4</sup>Here we are constantly comparing two DVH curves of the same structure on the same patient, so we always have  $n_A = n_B$ .

$$\text{where } \text{dist}(\mathcal{C}_A(i), \mathcal{C}_B(j(i))) = \sqrt{(d_i - \tilde{d}_{j(i)})^2 + (v_i - \tilde{v}_{j(i)})^2}$$

Here,  $j$  represents a (discrete) parametrization, and  $\text{dist}(\mathcal{C}_A(i), \mathcal{C}_B(j(i)))$  is the distance between points  $\mathcal{C}_A(i)$  and  $\mathcal{C}_B(j(i))$ .

One drawback of the Fréchet distance is its computational expense, particularly for structures with a large number of voxels. To mitigate this, we applied the Ramer–Douglas–Peucker algorithm for curve simplification [?]. We employed this algorithm with  $\epsilon = 0.05$ , and after testing on a subset of DVH curves, it was found to accelerate computations by a factor of 3-5, while the calculated Fréchet distance deviated by less than 0.5%. This method was therefore used in the results presented below.

**Hausdorff Distance** The Hausdorff distance is another commonly used metric for measuring the similarity between two curves [?]. It is defined as the greatest of the shortest distances between any point on one curve and the closest point on the other. Formally, let  $X$  and  $Y$  be two non-empty sets; the Hausdorff distance between  $X$  and  $Y$ , denoted  $d_{\text{Hausdorff}}(X, Y)$ , is given by:

$$d_{\text{Hausdorff}}(X, Y) = \sup_{x \in X} \inf_{y \in Y} \text{dist}(x, y)$$

where  $\text{dist}(x, y)$  represents the distance between points  $x$  and  $y$  (typically, the Euclidean distance).

In this study, we treat DVH (Dose-Volume Histogram) curves as sets of points in a two-dimensional space  $\mathbb{R}^2$ , using the Hausdorff distance to quantify their difference. Using the same notation for the DVH curves  $\mathcal{C}_A$  and  $\mathcal{C}_B$  as previously defined, the discrete Hausdorff distance is computed as:

$$d_{\text{Hausdorff}}(\mathcal{C}_A, \mathcal{C}_B) = \max_{i \in \llbracket 1, n_A \rrbracket} \min_{y \in \mathcal{C}_B} \text{dist}(\mathcal{C}_A(i), y)$$

where  $\mathcal{C}_B$  is represented by the set of points

$$\left\{ \left( (1 - \lambda)\tilde{d}_j + \lambda\tilde{d}_{j+1}, (1 - \lambda)\tilde{v}_j + \lambda\tilde{v}_{j+1} \right) \mid \lambda \in [0, 1], j \in \llbracket 1, n_B - 1 \rrbracket \right\}.$$

**Wasserstein Distance** The Wasserstein distance, also known as the Earth Mover’s Distance, is a metric used to quantify the difference between two probability distributions [?]. Formally, given two probability distributions  $\mu$  and  $\nu$  defined on a metric space  $X$ , the Wasserstein distance, denoted  $d_{\text{Wasserstein}}(\mu, \nu)$ , represents the infimum cost of transporting the mass of distribution  $\mu$  to match distribution  $\nu$ , where the transportation cost is determined by the distance metric  $\text{dist}$  on  $X$ . It is defined as:

$$d_{\text{Wasserstein}}(P, Q) = \inf_{\gamma \in \Gamma(\mu, \nu)} E_{(x, y) \sim \gamma} [\text{dist}(x, y)]$$

where  $\Gamma(\mu, \nu)$  represents the set of all possible joint distributions  $\gamma(x, y)$  with marginals  $\mu$  and  $\nu$ .

In our analysis, we treat DVH (Dose-Volume Histogram) curves as probability distributions and employ the Wasserstein distance to assess their differences. This metric has the distinct advantage of capturing both local and global variations between the curves, offering a more comprehensive comparison. However, it can be computationally demanding, particularly when dealing with DVHs of large anatomical structures.

**Kolmogorov-Smirnov Distance** Another distance metric commonly used to compare dose-volume histogram (DVH) curves is the Kolmogorov-Smirnov (KS) distance [?]. The KS distance measures the maximum vertical separation between two curves and is particularly well-suited for comparing non-parametric distributions, such as DVH curves.

Mathematically, let the two DVH curves be represented by functions  $f$  and  $g$ , mapping dose levels to volume ratios. The KS distance,  $d_{KS}$ , is then defined as:

$$d_{KS} = \sup_{x \in \mathbb{R}^+} |f(x) - g(x)|.$$

In the case of discrete DVH data,  $f$  and  $g$  are piecewise linear, continuous functions from  $\mathbb{R}^+$  to  $[0, 1]$ , with their values set to zero beyond the maximum dose level.

**Total Variation Distance** We propose a distance metric that computes the integral of the absolute difference between two DVH (dose-volume histogram) curves. This metric is straightforward to compute and provides a balanced measure of local and global differences between the curves [?]. Additionally, it is computationally efficient and well-suited for analyzing large structures with many voxels. This approach yielded the most consistent and clinically relevant results among the metrics tested. As such, we selected this distance measure for our analysis.

Traditionally, the total variation distance is defined as the integral of the absolute difference between two DVH curves. While the dose domain is theoretically unbounded, the volume domain is bounded between 0 and 100%. To avoid integrating over an unbounded dose domain, we opted to reverse the axes, placing dose on the  $y$ -axis and volume on the  $x$ -axis and subsequently integrating the absolute difference in dose over the volume range  $[0, 1]$ .

Mathematically, standard DVHs are described by  $V : \mathbb{R}^+ \rightarrow [0, 1]$ . For two DVHs  $V(d)$  and  $\tilde{V}(d)$ , the total variation distance is given by:

$$d_{\text{TotalVariation}} = \int_0^{+\infty} |V(d) - \tilde{V}(d)| dd$$

However, in our approach, we express DVHs with dose as a volume function, denoted  $D : [0, 1] \rightarrow \mathbb{R}^+$ . Thus, for two DVHs  $D(v)$  and  $\tilde{D}(v)$ , the total variation distance becomes:

$$d_{\text{TotalVariation}} = \int_0^1 |D(v) - \tilde{D}(v)| dv$$

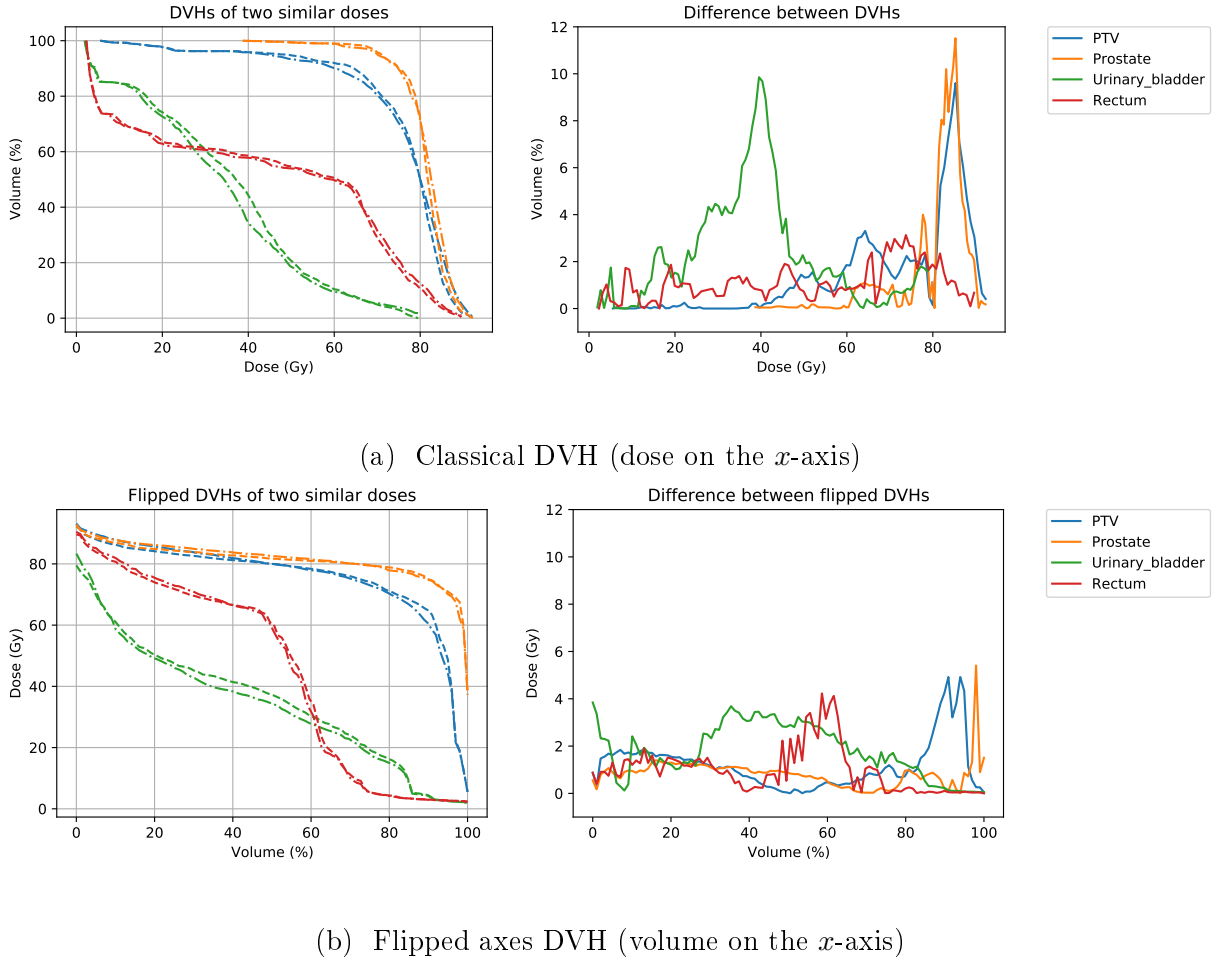


Figure 4.2: DVHs: Comparison of classical and flipped axes styles.

While the theoretical value of the integral remains unchanged, we prefer integrating over the finite volume domain  $[0, 1]$  instead of the unbounded dose domain  $\mathbb{R}^+ = [0, +\infty[$ . An illustration highlighting the differences between the classical DVH and the version with swapped  $x$ - and  $y$ -axes is presented in Figure 4.2. The two compared doses were optimized on the TG-119 phantom prostate case, using different weights (1 and 3) for the PTV objective.

As Figure 4.2 shows, the difference between DVHs exhibits less noise (fewer fluctuations) when the dose is on the  $x$ -axis. This observation suggests a reduction in numerical error, providing additional motivation to place the volume on the  $x$ -axis.

Computing the total variation distance is computationally efficient, requiring only  $\mathcal{O}(n_s)$  operations per structure, where  $n_s$  represents the number of voxels in the structure of interest,  $s$ . Overall, this method achieves a good balance between capturing local and global differences in DVH curves.



Figure 4.3: Pairwise distances between doses (with different distances calculation method)

## 4.1.2 Results

### 4.1.2.1 Dose Distances Comparison

We optimized each constraint with all weights initially set to 1 but sequentially increased one to 3, 10, and 100. This process resulted in 18 distinct dose distributions, which were compared using the distance metrics described earlier. We calculated the pairwise distances for each pair of doses, effectively constructing the adjacency matrix of a fully connected graph, where each optimized dose corresponds to a node. See Figure 4.3 for comparing the adjacency matrices.

Ideally, the distance metric should satisfy the following criteria:

- It should match the voxel-wise distance when the voxel-wise difference is small.
- It should remain small in cases where the voxel-wise distance is significant. However, the clinical significance of the two doses is similar, even if the doses are voxel-wise different.

From the pairwise distances shown in Figure 4.3, we make the following observations:

- The Fréchet and Hausdorff distances behave similarly to the voxel-wise distance, indicating that they are too sensitive. Thus, they are not suitable for our purpose.
- The Kolmogorov-Smirnov distance appears to degenerate, likely capturing noise due to numerical approximations in the DVH calculations. Therefore, it is also not suitable for our purpose.
- The Wasserstein and Total Variation distances produce more clinically relevant results. As a result, we chose to focus further analysis on these two metrics.

### 4.1.2.2 Link between Total Variation and Wasserstein

The adjacency matrices for the Wasserstein and Total Variation distances exhibit substantial similarity. This similarity is expected, as the two metrics are equivalent in this context, given that we employed the Earth Mover's Distance (Wasserstein distance with  $p = 1$ ). The Total Variation distance can be regarded as a particular case of the Wasserstein distance.

The Wasserstein distance, also known as the Earth Mover's Distance, provides a metric for

quantifying the distance between two probability distributions. Let  $X$  and  $Y$  be two distributions with cumulative distribution functions (CDFs)  $F$  and  $G$ , respectively. The Wasserstein distance between them is formally defined as:

$$W_p(F, G) = \inf_{\pi \in \Pi(F, G)} \left( \iint_{x,y \in \mathbb{R}^2} |x - y|^p d\pi(x, y) \right)^{1/p}$$

where  $\Pi(F, G)$  represents the set of all possible joint distributions with  $F$  and  $G$  as marginals.

In contrast, the Total Variation distance between the two curves  $F$  and  $G$  is defined as:

$$\text{TotalVariation}(F, G) = \int_{x \in \mathbb{R}} |F(x) - G(x)| dx$$

When the Wasserstein distance is computed with  $p = 1$ , it becomes equivalent to the Total Variation distance:

$$W_1(F, G) \equiv \text{TotalVariation}(F, G).$$

Thus, the only expected differences between these two distance metrics in our analysis should arise from numerical errors.

#### 4.1.2.3 Bounding of Total Variation and Voxel Distance

The Voxel Distance can bound the Total Variation distance. However, the reverse is impossible, as illustrated by the example in the introduction, where two doses exhibit nearly identical dose-volume histograms (DVHs) but significantly different voxel-wise distances.

In the following, we provide a bound for the Total Variation distance of a single DVH, which can be generalized to the sum of the Total Variation distances across all DVHs.

This proof demonstrates that while the Voxel Distance constrains the Total Variation distance, the converse does not hold, especially when voxel-wise variations do not translate to clinically meaningful differences in the global dose distribution.

We aim to compare two dose distributions on a structure,  $d$  and  $\tilde{d}$  (we suppose that  $d$  and  $\tilde{d}$  are lists containing only the values on the voxels of the structure).

#### Sorting lists

**Lemma 1.** *Let  $\dot{l}, l^* \in \mathbb{R}^n$ . Let  $\dot{l}$  be sorted and  $\dot{l}^* \in \mathbb{R}^n$  be sorted version of  $l^*$ . Then, we have:*

$$|\dot{l} - l^*| \geq |\dot{l} - \dot{l}^*|$$

*Proof.* Suppose  $a < b$  and  $c < d$ , and WLOG,  $a \leq c$ .

We have  $|a - d| = |a - c| + |c - d|$  so  $|a - d| + |b - c| = |a - c| + |c - d| + |b - c|$  using triangle inequality ( $|c - d| + |b - c| \geq |b - c|$ ):  $|a - d| + |b - c| \leq |a - c| + |b - d|$ .

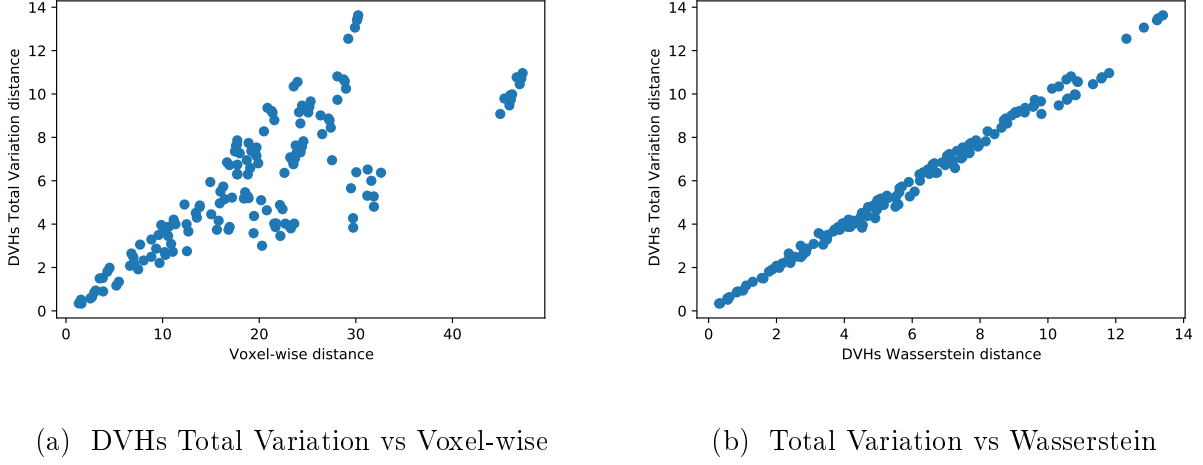


Figure 4.4: Comparing Distances

Thus, with  $\vec{l}$  sorted, swapping elements  $l_i$  and  $l_j$  ( $i < j$ ) of  $\vec{l}^*$  decreases  $|\vec{l} - \vec{l}^*|$  if  $l_i \geq l_j$ . Applying bubble sort on  $\vec{l}^*$ , we obtain  $\vec{l}^*$  doing only permutations satisfying the condition just stated.

Hence, we obtain  $|\vec{l} - \vec{l}^*| \geq |\vec{l} - \vec{l}^*|$  at the end of the bubble sort.  $\square$

**Corollary 1.** Let  $l, l^* \in \mathbb{R}^n$ . Let  $\vec{l}, \vec{l}^* \in \mathbb{R}^n$  be sorted version of  $l, l^*$ . Then:

$$|l - l^*| \geq |\vec{l} - \vec{l}^*|$$

*Proof.* The order in which we perform  $|l - l^*| = \sum_{k=1}^n |l_k - l_k^*|$  can be chosen, so  $|l - l^*| = \sum_{k=1}^n |l_{\sigma(k)} - l_{\sigma(k)}^*|$  (with  $\sigma$  a permutation of  $\llbracket 1, n \rrbracket$ ). Taking  $\sigma$  such that  $l_{\sigma(i)} \leq l_{\sigma(j)}$  for  $i < j$  and using lemma finishes the proof.  $\square$

**Proof Outline** Suppose the voxel-wise difference is  $\varepsilon$ -small (i.e.  $|d_i - \tilde{d}_i| < \varepsilon$ ). Then, the total variation of the unsorted vector doses is  $|\vec{d} - \tilde{\vec{d}}| < n_S \varepsilon$ . Let  $\vec{d}$  be sorted  $d$  and  $\tilde{\vec{d}}$  be sorted  $\tilde{d}$ . Then, by Corollary 1, we have:  $|\vec{d} - \tilde{\vec{d}}| \leq |\vec{d} - \tilde{\vec{d}}| < n_S \varepsilon$ .

Therefore, if  $d$  and  $\tilde{d}$  are sufficiently close,  $\varepsilon \rightarrow 0$  and  $|\vec{d} - \tilde{\vec{d}}| \rightarrow 0$ .

**Conclusion** Thus, voxel-wise very close doses distributions will also have close DVHs distances, which ensure DVHs distances are non-degenerative.

#### 4.1.2.4 Distances Distribution Comparison

**Comparing Total Variation and Voxel-wise** The bounding of the total variation DVH distance in terms of voxel-wise distance is clearly illustrated in Figure 4.4a, where a linear

upper bound can be observed in the scatter plot. However, specific pairs of doses are closer regarding DVH distance than initially anticipated based solely on voxel-wise comparisons. This observation underscores the need for a more nuanced analysis beyond voxel-wise comparison, as it may overlook clinically relevant similarities between dose distributions.

**Comparing Total Variation and Wasserstein** Figure 4.4b shows that the two DVH distances are nearly perfectly proportional. This result aligns with expectations, given that they are mathematically equivalent. The only difference lies in the integration axis in the total variation distance, which accounts for the small fluctuations observed, likely due to accumulated numerical error.

### 4.1.3 Discussion

In this section, we introduce a novel metric for comparing radiation doses. This metric offers the advantage of being insensitive to dose changes in certain regions, provided they are compensated in other regions, thus achieving the intended objective. This property makes the metric particularly useful in various applications, including dose mimicking and determining early stopping criteria for fluence map optimization.

Despite the advantages, this distance metric has certain limitations. A notable drawback is its inability to capture spatial dose distribution, which may pose challenges in specific cases. Pathological examples exist where two DVHs appear similar, but the clinical interpretation differs significantly. Other factors, such as the spatial distribution of the dose within the target volume or surrounding tissues, can play a pivotal role in the treatment's effectiveness.

For instance, two dose distributions might deliver the same high dose, with one distributed across several small regions and the other concentrated in a single large region. While the DVHs may appear identical, clinicians would interpret these two dose distributions differently. Such edge cases, however, are sporadic in clinical practice. Nonetheless, for critical cases, we recommend complementing this metric with voxel-invariant approaches and other techniques to evaluate the radiation doses comprehensively.

When comparing two distinct doses, a considerable distance between them may indicate a significant difference in the intensity or frequency of the treatment. However, this does not necessarily imply that one dose is superior. The effectiveness of a dose depends on several other factors, such as the individual patient's characteristics, medical history, and treatment response.

Therefore, relying solely on the distance between doses may not accurately assess which dose is more effective or clinically appropriate in a specific case. It is essential to account for all relevant factors when evaluating the efficacy of a treatment dose to ensure a comprehensive understanding.

Overall, the proposed dose comparison technique presents a promising tool for radiation dose evaluation. While it has certain limitations, it can serve as a valuable addition to the repertoire

of methods employed by radiation oncologists and medical physicists for optimizing treatment plans and improving patient outcomes. Complementing existing techniques offers an additional layer of analysis, contributing to more informed decision-making in clinical practice.

**Stop Criterion** Defining an adequate stopping criterion for the fluence map optimization process is a critical challenge in radiotherapy dose optimization. In clinical practice, dosimetrists often guide optimization, who may terminate the process when they are satisfied with the outcome. However, the need for fully automated optimization processes requires the establishment of systematic and objective stopping criteria. One potential approach is to compare the clinical effects of two dose distributions and stop when one optimization step does not change the clinical effect. This method can help evaluate different solutions and determine the optimal point to terminate the optimization process.

## 4.2 Network of Doses

### 4.2.1 Introduction

### 4.2.2 Radiotherapy

#### Dose Optimization Inputs

#### Dose Simulation

#### Dose-Volume Histograms

#### Evaluation of Doses

### 4.2.3 Methods

#### 4.2.3.1 Radiotherapy Dose Optimization

#### Simulation & Approximation

#### Physical Limitations

#### Mathematical Objective Function

#### MLC Fluence Discretization

#### Bixels Smoothness

Convexity

Multiple Plans Generation

Optimizer

4.2.3.2 Data

(Phantom) Patient

Dose normalization

4.2.3.3 Dose Clustering Techniques

Dose Distance

Community Detection

Evaluating Communities Split

4.2.4 Results

4.2.4.1 Doses Network

Graph Plots

DVH Plot

4.2.4.2 Dose Clustering Evaluation

4.2.5 Discussion

4.2.6 Conclusion

4.3 A Novel Framework for Multi-Objective Optimization and Robust Plan Selection Using Graph Theory (ESTRO 2024)



# Classical Dosimetry Automation

## Abstract

Lorem ipsum dolor sit amet, consectetuer adipiscing elit. Ut purus elit, vestibulum ut, placerat ac, adipiscing vitae, felis. Curabitur dictum gravida mauris. Nam arcu libero, nonummy eget, consectetuer id, vulputate a, magna. Donec vehicula augue eu neque. Pellentesque habitant morbi tristique senectus et netus et malesuada fames ac turpis egestas. Mauris ut leo. Cras viverra metus rhoncus sem. Nulla et lectus vestibulum urna fringilla ultrices. Phasellus eu tellus sit amet tortor gravida placerat. Integer sapien est, iaculis in, pretium quis, viverra ac, nunc. Praesent eget sem vel leo ultrices bibendum. Aenean faucibus. Morbi dolor nulla, malesuada eu, pulvinar at, mollis ac, nulla. Curabitur auctor semper nulla. Donec varius orci eget risus. Duis nibh mi, congue eu, accumsan eleifend, sagittis quis, diam. Duis eget orci sit amet orci dignissim rutrum.

Nam dui ligula, fringilla a, euismod sodales, sollicitudin vel, wisi. Morbi auctor lorem non justo. Nam lacus libero, pretium at, lobortis vitae, ultricies et, tellus. Donec aliquet, tortor sed accumsan bibendum, erat ligula aliquet magna, vitae ornare odio metus a mi. Morbi ac orci et nisl hendrerit mollis. Suspendisse ut massa. Cras nec ante. Pellentesque a nulla. Cum sociis natoque penatibus et magnis dis parturient montes, nascetur ridiculus mus. Aliquam tincidunt urna. Nulla ullamcorper vestibulum turpis. Pellentesque cursus luctus mauris.

---

5.1	Radiotherapy Dose Optimization via Clinical Knowledge Based Reinforcement Learning (AIME 2024) . . . . .	63
5.1.1	Introduction . . . . .	63
5.1.2	Materials and Methods . . . . .	63
5.1.3	Discussion . . . . .	63
5.1.4	Conclusion . . . . .	63
5.2	Clinically Dependent Fully Automatic Treatment Planning System (ASTRO 2024) . . . . .	63
5.2.1	Purpose / Objective . . . . .	63
5.2.2	Materials/Methods . . . . .	63
5.2.3	Results . . . . .	63
5.2.4	Conclusion . . . . .	63

---

## 5.1 Radiotherapy Dose Optimization via Clinical Knowledge Based Reinforcement Learning (AIME 2024)

### Abstract

#### 5.1.1 Introduction

#### 5.1.2 Materials and Methods

##### 5.1.2.1 Reinforcement Learning Reward

##### 5.1.2.2 Architecture

##### 5.1.2.3 Avoiding Off-Distribution

##### 5.1.2.4 Quantitative Results

##### 5.1.2.5 Qualitative Results

#### 5.1.3 Discussion

#### 5.1.4 Conclusion

### Appendix

Synthetic phantom patients

Clinical dose

Optimization

## 5.2 Clinically Dependent Fully Automatic Treatment Planning System (ASTRO 2024)

#### 5.2.1 Purpose / Objective

#### 5.2.2 Materials/Methods

#### 5.2.3 Results

#### 5.2.4 Conclusion



# Dosimetry Automation via Mimicking

## Abstract

Lorem ipsum dolor sit amet, consectetuer adipiscing elit. Ut purus elit, vestibulum ut, placerat ac, adipiscing vitae, felis. Curabitur dictum gravida mauris. Nam arcu libero, nonummy eget, consectetuer id, vulputate a, magna. Donec vehicula augue eu neque. Pellentesque habitant morbi tristique senectus et netus et malesuada fames ac turpis egestas. Mauris ut leo. Cras viverra metus rhoncus sem. Nulla et lectus vestibulum urna fringilla ultrices. Phasellus eu tellus sit amet tortor gravida placerat. Integer sapien est, iaculis in, pretium quis, viverra ac, nunc. Praesent eget sem vel leo ultrices bibendum. Aenean faucibus. Morbi dolor nulla, malesuada eu, pulvinar at, mollis ac, nulla. Curabitur auctor semper nulla. Donec varius orci eget risus. Duis nibh mi, congue eu, accumsan eleifend, sagittis quis, diam. Duis eget orci sit amet orci dignissim rutrum.

Nam dui ligula, fringilla a, euismod sodales, sollicitudin vel, wisi. Morbi auctor lorem non justo. Nam lacus libero, pretium at, lobortis vitae, ultricies et, tellus. Donec aliquet, tortor sed accumsan bibendum, erat ligula aliquet magna, vitae ornare odio metus a mi. Morbi ac orci et nisl hendrerit mollis. Suspendisse ut massa. Cras nec ante. Pellentesque a nulla. Cum sociis natoque penatibus et magnis dis parturient montes, nascetur ridiculus mus. Aliquam tincidunt urna. Nulla ullamcorper vestibulum turpis. Pellentesque cursus luctus mauris.

---

6.1	Dose-Volume Histograms Guided Deep Dose (SFPM 2024) . . . . .	67
6.1.1	Introduction . . . . .	67
6.1.2	Material and Methods . . . . .	67
6.1.3	Results . . . . .	67
6.1.4	Conclusions . . . . .	67
6.2	Attention Mechanism on Dose-Volume Histograms for Deep Dose Predictions (SFR0 2024) . . . . .	67
6.2.1	Introduction . . . . .	67
6.2.2	Material and Methods . . . . .	67
6.2.3	Results . . . . .	67
6.2.4	Conclusions . . . . .	67

---

## 6.1 Dose-Volume Histograms Guided Deep Dose (SFPM 2024)

6.1.1 Introduction

6.1.2 Material and Methods

6.1.3 Results

6.1.4 Conclusions

## 6.2 Attention Mechanism on Dose-Volume Histograms for Deep Dose Predictions (SFRO 2024)

6.2.1 Introduction

6.2.2 Material and Methods

6.2.3 Results

6.2.4 Conclusions



# Conclusion



# Perspectives



# Bibliography

- [1] Global cancer burden growing, amidst mounting need for services.
- [2] Stages of cancer.
- [3] Accuray. Precision<sup>®</sup>, 2024.
- [4] Erjona Bakiu, Ervis Telhaj, Elvisa Kozma, Ferdinand Ruçi, and Partizan Malkaj. Comparison of 3d crt and imrt treatment plans. *Acta informatica medica: AIM: journal of the Society for Medical Informatics of Bosnia & Herzegovina: casopis Drustva za medicinsku informatiku BiH*, 21(3):211–212, 2013. PMC3804479.
- [5] Beer. Bestimmung der absorption des rothen lichts in farbigen flüssigkeiten. *Annalen der Physik*, 162(5):78–88, 1852.
- [6] Somenath Bera and Vimal K Shrivastava. Analysis of various optimizers on deep convolutional neural network model in the application of hyperspectral remote sensing image classification. *International Journal of Remote Sensing*, 41(7):2664–2683, 2020.
- [7] JF Bonnans, Jean Charles Gilbert, C Lemaréchal, and Claudia Sagastizabal. *Numerical Optimization – Theoretical and Practical Aspects*. 01 2006.
- [8] Thomas Bortfeld. The number of beams in imrt—theoretical investigations and implications for single-arc imrt. *Physics in Medicine & Biology*, 55(1):83, nov 2009.
- [9] Roger Chammas, Cell Adhesion, and Cancer Group. Tumors as complex organs: are cancers manageable through the modification of their microenvironment? *BMC Proceedings*, 7(2):K16, Apr 2013.
- [10] Cyrus Chargari, Eric Deutsch, Pierre Blanchard, Sébastien Gouy, Hélène Martelli, Florent Guérin, Isabelle Dumas, Alberto Bossi, Philippe Morice, Akila N. Viswanathan, and Christine Haie-Meder. Brachytherapy: An overview for clinicians. *CA: A Cancer Journal for Clinicians*, 69(5):386–401, 2019.
- [11] Elizabeth Cohen-Jonathan, Eric J Bernhard, and W Gillies McKenna. How does radiation kill cells? *Current Opinion in Chemical Biology*, 3(1):77–83, 1999.
- [12] DKFZ. matrad, 2024.

- [13] Jingwei Duan, Mark Bernard, Laura Downes, Brooke Willows, Xue Feng, Waleed F. Mourad, William St Clair, and Quan Chen. Evaluating the clinical acceptability of deep learning contours of prostate and organs-at-risk in an automated prostate treatment planning process. *Medical Physics*, 49(4):2570–2581, 2022.
- [14] Elekta. One® | planning, 2024.
- [15] Robley D. Evans. *Compton Effect*, pages 218–298. Springer Berlin Heidelberg, Berlin, Heidelberg, 1958.
- [16] John D. Fenwick and Juan Pardo-Montero. Numbers of beam angles required for near-optimal imrt: Theoretical limits and numerical studies. *Medical Physics*, 38(8):4518–4530, 2011.
- [17] Roger Fletcher and Chengian Xu. Hybrid methods for nonlinear least squares. *IMA Journal of Numerical Analysis*, 7(3):371–389, 1987.
- [18] Nicholas Hardcastle, Wolfgang A. Tomé, Kerwyn Foo, Andrew Miller, Martin Carolan, and Peter Metcalfe. Comparison of prostate imrt and vmat biologically optimised treatment plans. *Medical Dosimetry*, 36(3):292–298, 2011.
- [19] Haihua He, Tangpeng Xu, Ping Li, Guohua Jia, Xiangpan Li, and Qibin Song. Anti-pd-1 immunotherapy combined with stereotactic body radiation therapy and gm-csf as salvage therapy in a pd-l1-positive patient with refractory metastatic thyroid hürthle cell carcinoma: A case report and literature review. *Frontiers in Oncology*, 11, 2021.
- [20] Magnus R. Hestenes and Eduard Stiefel. Methods of conjugate gradients for solving linear systems. *Journal of research of the National Bureau of Standards*, 49:409–435, 1952.
- [21] Geoffrey Hinton, Nitish Srivastava, and Kevin Swersky. Neural networks for machine learning lecture 6a overview of mini-batch gradient descent. *Cited on*, 14(8):2, 2012.
- [22] J.B. Hiriart-Urruty and C. Lemaréchal. *Fundamentals of Convex Analysis*. Grundlehren Text Editions. Springer Berlin Heidelberg, 2012.
- [23] L R Holsti. Development of clinical radiotherapy since 1896. *Acta Oncol*, 34(8):995–1003, 1995.
- [24] Haakon Hop, Vance L. Trudeau, and Mark Graham. Spawning energetics of arctic cod (*boreogadus saida*) in relation to seasonal development of the ovary and plasma sex steroid levels. *Canadian Journal of Fisheries and Aquatic Sciences*, 52(3):541–550, 1995.
- [25] Hyun Do Huh and Seonghoon Kim. History of radiation therapy technology. *Progress in Medical Physics*, 31(3):124–134, Sep 2020.
- [26] Christian Wittekind James D. Brierley, Mary K. Gospodarowicz. *TNM Classification of Malignant Tumours, 8th Edition*. Wiey Blackwell, 8th (2016) edition. TNM Classification of Malignant Tumours eighth edition provides the latest, internationally agreed-upon standards to describe and categorize cancer stage.

- [27] Robert Jeraj, Thomas R. Mackie, John Balog, Gustavo Olivera, Dave Pearson, Jeff Kapatoes, Ken Ruchala, and Paul Reckwerdt. Radiation characteristics of helical tomotherapy. *Medical Physics*, 31(2):396–404, 2004.
- [28] Warren Kilby, Michael Naylor, John R. Dooley, Calvin R. Maurer, and Sohail Sayeh. 2 - a technical overview of the cyberknife system. In Mohammad H. Abedin-Nasab, editor, *Handbook of Robotic and Image-Guided Surgery*, pages 15–38. Elsevier, 2020.
- [29] Young Woo Kim, Simon Biggs, and Elizabeth Claridge Mackonis. Investigation on performance of multiple ai-based auto-contouring systems in organs at risks (oars) delineation. *Physical and Engineering Sciences in Medicine*, 47(3):1123–1140, Sep 2024.
- [30] Diederik P. Kingma and Jimmy Ba. Adam: A method for stochastic optimization, 2017.
- [31] Eric A. Klein, Jay Ciezki, Patrick A. Kupelian, and Arul Mahadevan. Outcomes for intermediate risk prostate cancer: Are there advantages for surgery, external radiation, or brachytherapy? *Urologic Oncology: Seminars and Original Investigations*, 27(1):67–71, 2009. Proceedings: Annual Meeting of the Society of Urologic Oncology/Society for Basic Urologic Research (May 2007).
- [32] RaySearch Laboratories. Raystation, 2024.
- [33] Dong C. Liu and Jorge Nocedal. On the limited memory bfgs method for large scale optimization. *Mathematical Programming*, 45(1):503–528, Aug 1989.
- [34] Liyuan Liu, Haoming Jiang, Pengcheng He, Weizhu Chen, Xiaodong Liu, Jianfeng Gao, and Jiawei Han. On the variance of the adaptive learning rate and beyond, 2021.
- [35] Shu-Zheng Liu. Nonlinear dose-response relationship in the immune system following exposure to ionizing radiation: Mechanisms and implications. *Nonlinearity in Biology, Toxicology, Medicine*, 1(1):15401420390844483, 2003. PMID: 19330113.
- [36] T. Rockwell Mackie, John Balog, Ken Ruchala, Dave Shepard, Stacy Aldridge, Ed Fitchard, Paul Reckwerdt, Gustavo Olivera, Todd McNutt, and Minesh Mehta. Tomotherapy. *Seminars in Radiation Oncology*, 9(1):108–117, Jan 1999.
- [37] Luis A. Maduro Bustos, Abhirup Sarkar, Laura A. Doyle, Kelly Andreou, Jodie Noonan, Diana Nurbagandova, SunJay A. Shah, Omoruyi Credit Irabor, and Firas Mourtada. Feasibility evaluation of novel ai-based deep-learning contouring algorithm for radiotherapy. *Journal of Applied Clinical Medical Physics*, 24(11):e14090, 2023.
- [38] Francois Eschwège Maurice Tubiana. Conformal radiotherapy and intensity-modulated radiotherapy: Clinical data. *Acta Oncologica*, 39(5):555–567, 2000. PMID: 11093364.
- [39] Hans-Georg Menzel. The ICRU report 83: prescribing, recording and reporting photon-beam intensity-modulated radiation therapy (IMRT). 10(1), January 2010.

- [40] Dinesh Kumar Mynampati, Ravindra Yaparpalvi, Linda Hong, Hsiang-Chi Kuo, and Dennis Mah. Application of aapm tg 119 to volumetric arc therapy (vmat). *Journal of Applied Clinical Medical Physics*, 13(5):108–116, 2012.
- [41] Toshiaki Nakano, Xu Xu, Amir M.H. Salem, Mahmoud I. Shoulkamy, and Hiroshi Ide. Radiation-induced dna–protein cross-links: Mechanisms and biological significance. *Free Radical Biology and Medicine*, 107:136–145, 2017. Oxidative DNA Damage & Repair.
- [42] Liming XU Ning GE, Fuci CHEN. Comparison between sliding window and step and shoot. 6.
- [43] Jorge Nocedal and Stephen J. Wright. *Numerical optimization*. Springer series in operations research and financial engineering. Springer, New York, NY, 2nd ed. edition, 2006. MAB0014.001: M 11.0268.
- [44] Barnabas Poczos and Ryan Tibshirani. *Convex Optimization*.
- [45] Enzhuo M. Quan, Xiaoqiang Li, Yupeng Li, Xiaochun Wang, Rajat J. Kudchadker, Jennifer L. Johnson, Deborah A. Kuban, Andrew K. Lee, and Xiaodong Zhang. A comprehensive comparison of imrt and vmat plan quality for prostate cancer treatment. *International Journal of Radiation Oncology\*Biology\*Physics*, 83(4):1169–1178, 2012.
- [46] Martin A. Riedmiller and Heinrich Braun. Rprop - a fast adaptive learning algorithm. 1992.
- [47] Humberto Rocha, Joana Matos Dias, Tiago Ventura, Brígida da Costa Ferreira, and Maria do Carmo Lopes. Beam angle optimization in imrt: are we really optimizing what matters? *International Transactions in Operational Research*, 26(3):908–928, 2019.
- [48] R Roots, G Kraft, and E Gosschalk. The formation of radiation-induced dna breaks: The ratio of double-strand breaks to single-strand breaks. *International Journal of Radiation Oncology\*Biology\*Physics*, 11(2):259–265, 1985.
- [49] G. Scholes. Radiation effects on dna. the silvanus thompson memorial lecture, april 1982. *British Journal of Radiology*, 56(664):221–231, 05 2014.
- [50] Z. Somosy. Radiation response of cell organelles. *Micron*, 31(2):165–181, 2000.
- [51] Patricia S Steeg. Tumor metastasis: mechanistic insights and clinical challenges. *Nat. Med.*, 12(8):895–904, aug 2006.
- [52] Silvia Strolin, Miriam Santoro, Giulia Paolani, Ilario Ammendolia, Alessandra Arcelli, Anna Benini, Silvia Bisello, Raffaele Cardano, Letizia Cavallini, Elisa Deraco, Costanza Maria Donati, Erika Galletta, Andrea Galuppi, Alessandra Guido, Martina Ferrioli, Viola Laghi, Federica Medici, Maria Ntreta, Natalya Razganiayeva, Giambattista Siepe, Giorgio Tolento, Daria Vallerossa, Alice Zamagni, Alessio Giuseppe Morganti, and Lidia Strigari. How smart is artificial intelligence in organs delineation? testing a CE and

- FDA-approved Deep-Learning tool using multiple expert contours delineated on planning CT images. *Front. Oncol.*, 13:1089807, March 2023.
- [53] Ange Tato and Roger Nkambou. Improving adam optimizer. 2018.
  - [54] Juliette Thariat, Jean-Michel Hannoun-Levi, Arthur Sun Myint, Te Vuong, and Jean-Pierre Gérard. Past, present, and future of radiotherapy for the benefit of patients. *Nature Reviews Clinical Oncology*, 10(1):52–60, Jan 2013.
  - [55] Claire Vanpouille-Box, Karsten A. Pilones, Erik Wennerberg, Silvia C. Formenti, and Sandra Demaria. In situ vaccination by radiotherapy to improve responses to anti-ctla-4 treatment. *Vaccine*, 33(51):7415–7422, 2015.
  - [56] Varian. Eclipse™ treatment planning system. Online.
  - [57] Varian. Eclipse™ 2024.
  - [58] Richard C. Walshaw, Jamie Honeychurch, Ananya Choudhury, and Timothy M. Illidge. Toll-like receptor agonists and radiation therapy combinations: An untapped opportunity to induce anticancer immunity and improve tumor control. *International Journal of Radiation Oncology\*Biology\*Physics*, 108(1):27–37, 2020. Radiation Therapy and the Immune Response.
  - [59] Jin-Song Wang, Hai-Juan Wang, and Hai-Li Qian. Biological effects of radiation on cancer cells. *Mil. Med. Res.*, 5(1), dec 2018.
  - [60] Esther Witsch, Michael Sela, and Yosef Yarden. Roles for growth factors in cancer progression. *Physiology*, 25(2):85–101, 2010. PMID: 20430953.
  - [61] Dandan Xu, Guowen Li, Hongfei Li, and Fei Jia. Comparison of imrt versus 3d-crt in the treatment of esophagus cancer. *Medicine*, 96(31):e7685, Aug 2017.
  - [62] Matthew D. Zeiler. Adadelta: An adaptive learning rate method, 2012.
  - [63] Lina Zhao, Shouhao Zhou, Peter Balter, Chan Shen, Daniel R Gomez, James D Welsh, Steve H Lin, and Joe Y Chang. Planning target volume D95 and mean dose should be considered for optimal local control for stereotactic ablative radiation therapy. *Int. J. Radiat. Oncol. Biol. Phys.*, 95(4):1226–1235, July 2016.